Basic Research in Cardiology (2023) 118:14
https://doi.org/10.1007/s00395-022-00973-0

ORIGINAL CONTRIBUTION

Electrophysiological and calcium-handling development during long-term culture of human-induced pluripotent stem cell-derived cardiomyocytes

Fitzwilliam Seibertz[1,2,3] · Henry Sutanto[4] · Rebekka Dülk[1,2] · Julius Ryan D. Pronto[1,2] · Robin Springer[1,2] · Markus Rapedius[5] · Aiste Liutkute[1,2,3] · Melanie Ritter[1,2] · Philipp Jung[1,2] · Lea Stelzer[1,2] · Luisa M. Hüsgen[1,2] · Marie Klopp[1,2] · Tony Rubio[1,2] · Funsho E. Fakuade[1,2,3] · Fleur E. Mason[1,2] · Nico Hartmann[6] · Steffen Pabel[7] · Katrin Streckfuss-Bömeke[2,6,8] · Lukas Cyganek[2,3,6] · Samuel Sossalla[2,6,7] · Jordi Heijman[4] · Niels Voigt[1,2,3]

Received: 13 September 2022 / Revised: 13 December 2022 / Accepted: 15 December 2022 / Published online: 5 April 2023

Abstract

Human-induced pluripotent stem cell-derived cardiomyocytes (hiPSC-CMs) are increasingly used for personalised medicine and preclinical cardiotoxicity testing. Reports on hiPSC-CM commonly describe heterogenous functional readouts and underdeveloped or immature phenotypical properties. Cost-effective, fully defined monolayer culture is approaching mainstream adoption; however, the optimal age at which to utilise hiPSC-CM is unknown. In this study, we identify, track and model the dynamic developmental behaviour of key ionic currents and Ca^{2+}-handling properties in hiPSC-CM over long-term culture (30–80 days). hiPSC-CMs > 50 days post differentiation show significantly larger $I_{Ca,L}$ density along with an increased $I_{Ca,L}$-triggered Ca^{2+}-transient. I_{Na} and I_{K1} densities significantly increase in late-stage cells, contributing to increased upstroke velocity and reduced action potential duration, respectively. Importantly, our in silico model of hiPSC-CM electrophysiological age dependence confirmed I_{K1} as the key ionic determinant of action potential shortening in older cells. We have made this model available through an open source software interface that easily allows users to simulate hiPSC-CM electrophysiology and Ca^{2+}-handling and select the appropriate age range for their parameter of interest. This tool, together with the insights from our comprehensive experimental characterisation, could be useful in future optimisation of the culture-to-characterisation pipeline in the field of hiPSC-CM research.

Keywords Stem cell · Calcium handling · Maturation · Ion channel · Action potential · Cardiovascular

Fitzwilliam Seibertz and Henry Sutanto have contributed equally to this work.

✉ Jordi Heijman
jordi.heijman@maastrichtuniversity.nl

✉ Niels Voigt
niels.voigt@med.uni-goettingen.de

1 Institute of Pharmacology and Toxicology, University Medical Center Göttingen, Georg-August University Göttingen, Universitätsmedizin Göttingen, Robert-Koch-Straße 40, 37075 Göttingen, Germany

2 DZHK (German Center for Cardiovascular Research), Partner Site Göttingen, Göttingen, Germany

3 Cluster of Excellence "Multiscale Bioimaging: From Molecular Machines to Networks of Excitable Cells" (MBExC), University of Göttingen, Göttingen, Germany

4 Department of Cardiology, Cardiovascular Research Institute Maastricht, Faculty of Health, Medicine and Life Sciences, Maastricht University, Universiteitssingel 50, 6229 ER Maastricht, The Netherlands

5 Nanion Technologies GmbH, Munich, Germany

6 Clinic for Cardiology and Pneumology, University Medical Center Göttingen, Georg-August University Göttingen, Göttingen, Germany

7 Department of Internal Medicine II, University Medical Center Regensburg, Regensburg, Germany

8 Institute of Pharmacology and Toxicology, University of Würzburg, Würzburg, Germany

Introduction

Human-induced pluripotent stem cell-derived cardiomyocytes (hiPSC-CMs) show immense promise for the cost-effective development of personalised medicine and the streamlining of preclinical cardiotoxicity testing [1]. Derived from blood or minimally invasive patient biopsies, in vitro hiPSC-CM constructs preserve patient-specific genotypes, are highly scalable and avoid the practical and ethical pitfalls associated with primary human tissue culture and animal experimentation [79]. hiPSC-CM technology has contributed to the emergence of initiatives such as the comprehensive in vitro proarrhythmia assay (CiPA) approach where multimodal examinations of drug responses aim to provide a more robust assessment of proarrhythmic risk [17, 60].

At present, in vitro hiPSC-CM technology is limited both by a persistent state of phenotypic immaturity and highly heterogenous readouts of electrophysiological function. The latter could simply reflect the genetic variability inherent in the general population; however, even hiPSC-CM derived from the same donor and within the same cell-line can demonstrate large phenotypic variability [13]. Variability could arise from numerous sources including differentiation methods, plating densities, or indeed the age at which the hiPSC-CM construct is assayed. hiPSC-CM morphology and function can evolve over long culture periods [49]. Functional expression of major ionic currents including the transient-outward K^+ current (I_{to}) and L-type Ca^{2+} current ($I_{Ca,L}$) increases in human embryonic stem cell-derived cardiomyocytes (hESC-CM) cultured for several weeks [64], recapitulating electrophysiological embryonic development described in animal models [30]. In hiPSC-CM, action potential (AP) characteristics have also been reported to change haphazardly during long culture periods, prompting the notion of temporal fluidity in the dominant cardiac subtype within in vitro cultures [3]. These findings suggest the presence of complex nonlinear changes in ion channel characteristics throughout cell culture. Although cardiomyocyte Ca^{2+}-handling is essential for excitation–contraction coupling and plays a major role in arrhythmogenesis [67], a comparative readout of Ca^{2+}-handling has yet to be reported in hiPSC-CM over 30 days post differentiation [11, 27, 48]. There is little standardisation of the ages at which hiPSC-CMs are employed for drug screening or modelling purposes [3, 11]. We hypothesise that developmental processes during long-term hiPSC-CM culture may contribute to the phenotypic variability frequently reported within and between laboratories. Therefore, the present work characterises the passive maturation of hiPSC-CM electrophysiology and Ca^{2+}-handling during long-term culture. Finally, to evaluate whether our experimentally observed age-dependent changes in Ca^{2+}-handling parameters and major ionic currents are sufficient to explain the experimentally acquired AP characteristics, we have integrated our experimental data into an in silico framework based on recent hiPSC-CM-specific in silico models of cardiac cellular electrophysiology [36, 40, 54, 55].

Methods

Further details of all methods can be found in the Online Data Supplement.

Somatic cell reprogramming and cardiac differentiation

hiPSC cell line UMGi014-C clone 14 (isWT1.14) was derived from the dermal fibroblasts of a healthy male donor (31 years). They were cultured in feeder-free conditions using the integration-free CytoTune iPS 2.0 Sendai Reprogramming Kit (Thermo Fisher Scientific) with reprogramming factors OCT4, KLF4, SOX2, c-MYC. Previously published pluripotency and karyotype analysis of this line revealed no abnormalities or chromosomal instability [59]. Experimental protocols were approved by the ethics committee of the University Medical Center Göttingen (10/9/15). Directed feeder-free cardiac differentiation was achieved via canonical WNT modulation with small-molecules CHIR and IWP2, followed by metabolic selection with lactate as previously described [19, 39]. Day-3 (d-3) indicates final passaging whilst day 0 (d0) marks the onset of differentiation with WNT stimulation.

Cellular preparation

Between d27 and d30, purified hiPSC-CMs were digested with TrypLE (Thermo Fisher Scientific) and sparsely plated on 1:60 Matrigel-coated borosilicate glass 10 mm #0 round coverslips at a density of 15,000 cells/cm^2. Cells were incubated at 37 °C in 5% CO_2 and maintained every 2–3 days with a culture medium containing RPMI 1640 supplemented with B-27 (both Thermo Fisher Scientific). Cellular beating rate was routinely measured by photometric capture at × 40 magnification with a Retiga R6™ CCD camera mounted on an inverted microscope. Recordings were taken at 13 frames per second and analysed offline using the MUSCLEMOTION™ plugin on ImageJ [62]. For experimentation, coverslips were removed from their media and inserted directly into a heated bath chamber mounted on the stage of an inverted epifluorescence microscope. The differentiation and preparation process is outlined in Fig. 1a.

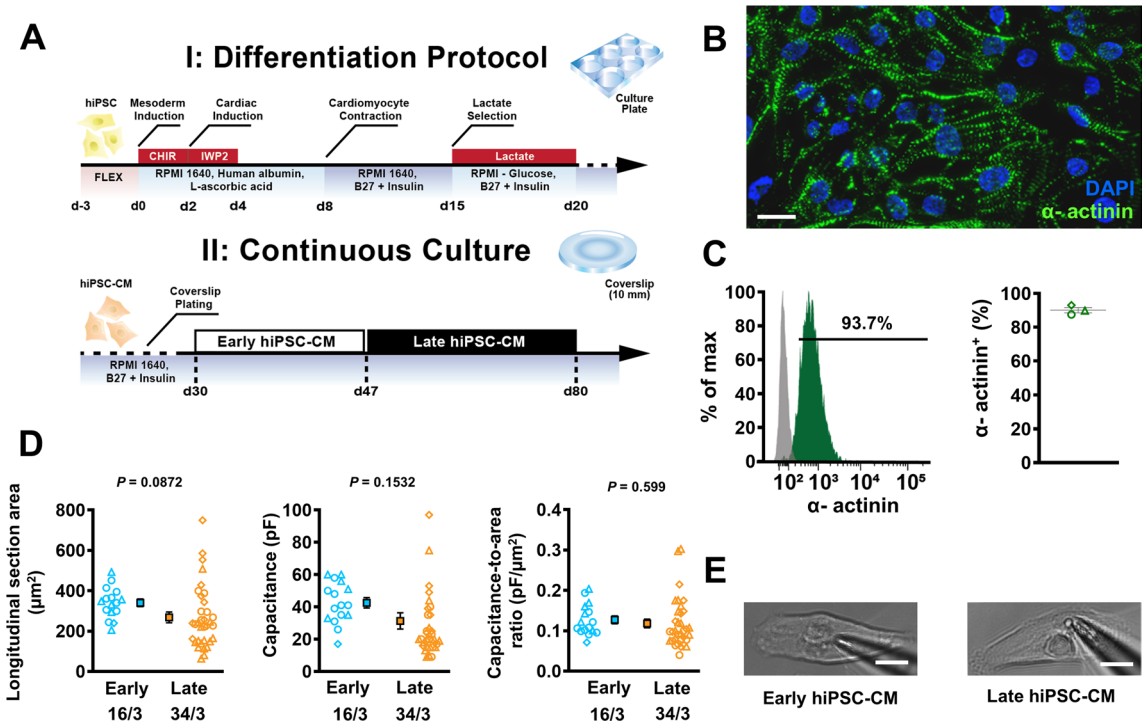

Fig. 1 Overview of human induced pluripotent stem cell-derived cardiomyocytes (hiPSC-CM) differentiation. **A** Schematic overview of the differentiation protocol utilised in this study (upper), and the process of long-term continuous culture on glass coverslips (lower). Early (young) hiPSC-CM underwent experimentation between 30 and 46 days after differentiation whilst late (old) hiPSC-CM were measured between day 47 to 80. **B** Immunofluorescent staining of hiPSC-CM at d29. **C** Flow cytometry analysis of hiPSC-CM at d29. **D** Longitudinal section area of early and late hiPSC-CM (left), corresponding cell capacitance (middle) and T-tubule density (right), estimated through a ratio of capacitance to longitudinal section area of each cell. **E** Representative photomicrographs of early (left) and late (right) hiPSC-CM. Scale bar represents 10 µm. Data are mean ± SEM. Symbols represent separate differentiations. *n*/*N* = number of hiPSC-CM/differentiation

Electrophysiological recordings

Whole-cell ruptured-patch techniques were employed to measure membrane currents in single, isolated early (d30–d46) and late (d47–d80) stage hiPSC-CMs. $I_{Ca,L}$ and intracellular Ca^{2+} were measured simultaneously at 0.5 Hz with a voltage-clamp protocol consisting of a 100-ms ramp to − 40 mV (inactivating the fast Na^+ current; I_{Na}) followed by a 100-ms depolarising test-pulse to + 10 mV, as previously described [15, 77]. For current voltage (I–V) curves, the test pulse was altered from − 40 to + 60 mV with 5 mV steps. Bath solution contained (in mmol/L): $CaCl_2$ 2, glucose 10, HEPES 10, KCl 4, $MgCl_2$ 1, NaCl 140, probenecid 2; pH = 7.35. 4-aminopyridine (5 mmol/L) and $BaCl_2$ (0.1 mmol/L) were added to block K^+ currents [8, 73, 74, 78]. Pipette solution contained (in mmol/L): Fluo-3 pentapotassium salt 0.1, EGTA 0.02, GTP-Tris 0.1, HEPES 10, K-aspartate 92, KCl 48, Mg-ATP 1, Na_2-ATP 4; pH = 7.2. Sarcoplasmic reticulum (SR) Ca^{2+} content was assessed through integration of the Na^+/Ca^{2+} exchanger-mediated current (I_{NCX}) during perfusion with 10 mmol/L caffeine.

Peak I_{Na} was measured in a bath solution containing (in mmol/L): NaCl 5, HEPES 10, $MgCl_2$ 1, CsCl 10, glucose 10, $CaCl_2$ 0.5, and TEA-Cl 120 (pH = 7.4, adjusted with CsOH). A voltage-clamp protocol was applied consisting of a holding potential at − 80 mV, followed by a 1000-ms pre-pulse step at − 110 mV (to increase availability of Na^+ channels), and then 30-ms steps from − 80 to + 20 mV for I–V curves. Late Na^+ current ($I_{Na,L}$) measurements were conducted with a bath solution containing (in mmol/L): NaCl 120, HEPES 10, $MgCl_2$ 1, CsCl 10, glucose 10 and $CaCl_2$ 0.5 (pH = 7.4, adjusted with CsOH). A voltage-clamp protocol was applied consisting of a holding potential of − 120 mV, followed by a 5-ms activating step to + 50 mV and a 300-ms step to − 30 mV to assess $I_{Na,L}$. Pipette solution for both I_{Na} and $I_{Na,L}$ measurements contained (in mmol/L): NaCl 5, EGTA 10, GTP-Tris 0.4, HEPES 10, Mg-ATP 4, CsCl 20, $CaCl_2$ 3, Cs-Methansulfonate 90, pH = 7.2.

Delayed rectifier (rapid component; I_{Kr}) tail currents were measured using a high-performance automated patch clamp system (SyncroPatch 384; Nanion Technologies GmbH) with a voltage-clamp protocol consisting of a holding potential of − 80 mV followed by a 2-s step to

60 mV with steps of 10 mV for I–V acquisition. Bath solution contained (in mmol/L): CsCl 144, $CaCl_2$ 2, $MgCl_2$ 2, glucose 5, HEPES 10 (pH = 7.4 adjusted with CsOH). Pipette solution contained (in mmol/L) CsCl 20, EGTA 10, HEPES 10, CsF 110 (pH = 7.2 adjusted with CsOH) in accordance with a recently published protocol [26]. Cs^+ was used as a charge carrier due to its selectivity for the hERG channel [65].

Basal inward-rectifier K^+ current (I_{K1}) was measured at 0.5 Hz with a ramp pulse from − 100 to + 40 mV at 0.5 Hz while superfusing a modified Tyrode's bath solution containing (mmol/L): NaCl 120, KCl 20, $MgCl_2$ 1, $CaCl_2$ 2, glucose 10, HEPES 10, pH = 7.4. Pipette solution contained (in mmol/L): EGTA 0.02, GTP-Tris 0.1, HEPES 10, K-aspartate 92, KCl 48, Mg-ATP 1, Na_2-ATP 4; pH = 7.2. I_{K1} was identified as Ba^{2+} (1 mmol/L)-sensitive current as previously described [76].

APs were measured in current-clamp configuration at 0.5 Hz in bath solution containing (in mmol/L) the following: $CaCl_2$ 2, glucose 10, HEPES 10, KCl 4, $MgCl_2$ 1, NaCl 140; pH = 7.35. Pipette solution contained (in mmol/L): EGTA 0.02, GTP-Tris 0.1, HEPES 10, K-aspartate 92, KCl 48, Mg-ATP 1, Na_2-ATP 4; pH = 7.2. Mean holding currents were − 0.86 ± 0.13 pA/pF for early hiPSC-CM and − 1.05 ± 0.16 pA/pF for late hiPSC-CM ($P = 0.3651$).

All electrophysiological experiments were carried out at 37 °C, except for I_{Na}, $I_{Na,L}$ and I_{Kr} which were measured at room temperature. Seal resistances were 3–6 GΩ. Borosilicate glass pipettes with tip resistances of 2–7 MΩ were used for voltage clamp experiments. High resistance borosilicate glass pipettes (5–10 MΩ) were used for current clamp experiments. All current recordings (except for I_{Kr}) were acquired using an Axopatch 200B microelectrode amplifier and analysed using pClamp-Software V 10.7 (both from Axon Instruments Inc., Foster City, USA). Membrane currents were corrected for membrane capacitance and expressed in pA/pF. Action potentials were acquired using a HEKA amplifier and HEKA patchmaster software and analysed using Lab Chart 7 (AD instruments, Otago, New Zealand).

Simultaneous intracellular Ca^{2+} measurements

$[Ca^{2+}]_i$ of single, isolated early- and late-stage hiPSC-CM was measured using the fluorescent Ca^{2+} indicator fluo-3-acetoxymethyl ester (Fluo-3-AM, 10 µmol/L, 10 min loading, 30 min de-esterification, $\lambda_{Ex} = 488$ nm, $\lambda_{Em} = 535$ nm) during simultaneous $I_{Ca,L}$ measurement at 37 °C as previously described [77]. Fluorescence emission was collected with a photomultiplier optimised for high-speed signal capture (10 kHz). Emission was correlated to $[Ca^{2+}]_i$ with the formula $[Ca^{2+}]_i = K_d\,[F/(F_{max} - F)]$. Here, K_d represents the dissociation constant of Fluo-3 (864 nmol/L), F denotes Fluo-3 fluorescence, and F_{max} describes Ca^{2+}-saturated fluorescence obtained through cellular laceration at the end of each experiment [15].

Molecular biology studies

Early and late hiPSC-CM were trypsinised and cellular membranes were isolated by differential centrifugation and then solubilized at 1 mg/ml of total protein in solubilisation buffer. Ca^{2+}-handling proteins SERCA2a and NCX1, as well as expression of Kir2.1 were analysed with immunoblotting techniques. (LI-COR Biotechnology, US). Antibodies are outlined in Online Table S1. Immunofluorescent screening stained for nuclear and sarcomeric proteins using hiPSC-CM (d29) fixed in 4% PFA and permeabilised in 0.1% Triton X-100 with an AxioObserver A1 fluorescence microscope (Carl Zeiss, Jena, Germany). Flow cytometry utilised trypsinised, fixed and permeabilised hiPSC-CM (d29). Cells were screened using the LSRII flow cytometer (BD Biosciences, US).

Computational modelling

The state-of-the-art in silico hiPSC-CM model by Kernik et al. [36] formed the basis for our simulations. The model was implemented in Myokit [9] and model parameters were adjusted to reproduce experimental data from early- or late-stage hiPSC-CM obtained in the present study (Online Table S2). The model age was set to 30 days for early-stage hiPSC-CM and 50 days for late-stage hiPSC-CM. For optimisation of I_{K1}, 40 days and 60 days were used, based on the maturity levels of the experimental data. Finally, we interpolated the parameters obtained for the early- and late-stage hiPSC-CM models to obtain parameter values as a function of age (Online Table S2, right columns). Linear functions were used for interpolation whenever possible. Alternatively, Hill functions were employed to prevent unphysiological values (e.g., negative membrane capacitance) at advanced age. AP simulations were performed and the steady-state AP following 1000 beats of prepacing was used for analysis in the presence of 0.2 pA/pF hyperpolarising current injected to suppress hiPSC-CM automaticity. The model code is freely accessible at www.github.com/jordiheijman. The installation guide for the induced pluripotent stem cell-derived maturity evaluator (iMATURE) is available in the Online Supplement.

Statistical analysis

Data are reported as mean ± SEM and *n*-numbers as *n*/*N*, where n indicates number of hiPSC-CM studied from N

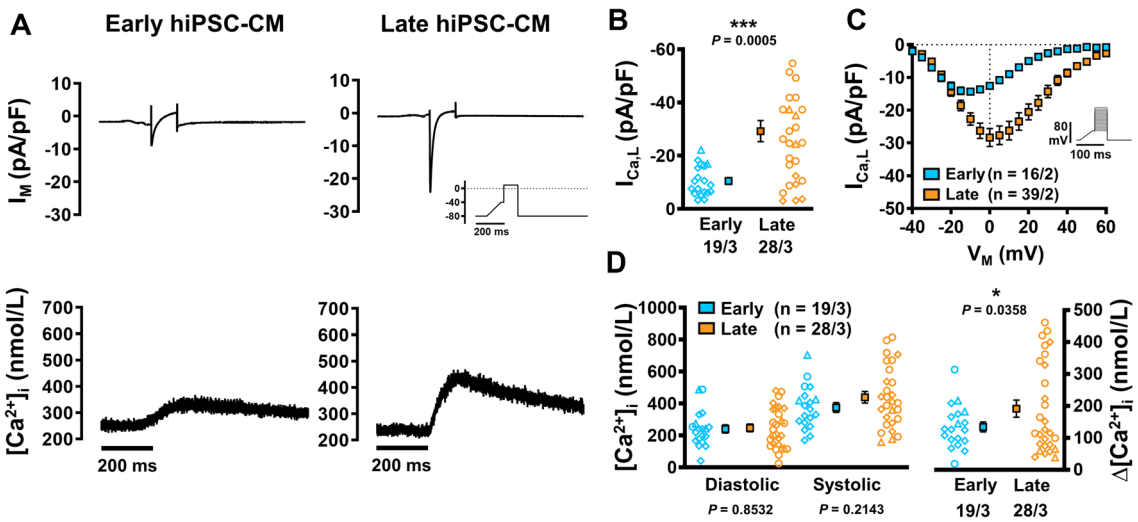

Fig. 2 $I_{Ca,L}$-triggered Ca^{2+} transients (CaT) in isolated early and late human induced pluripotent stem cell-derived cardiomyocytes (hiPSC-CM). **A** Representative simultaneous recordings of $I_{Ca,L}$ (upper) and triggered CaT (lower) in early (left) and late hiPSC-CM (right). Inset: voltage-clamp protocol. **B** Peak $I_{Ca,L}$. **C** Current–voltage relationship curve for $I_{Ca,L}$. **D** Diastolic and systolic $[Ca^{2+}]_i$ (left) and resulting CaT-amplitude (right). Data are mean ± SEM. $^*P<0.05$ $^{***}P<0.001$ versus early hiPSC-CM culture by Welch's t test or Student's t test (D left). Symbols represent separate differentiations. *n*/*N* = number of hiPSC-CM/differentiation

differentiations, unless otherwise stated. Analyses were carried out with Prism 8 software (Graphpad, San Diego, USA). Normality of the data distribution was assessed using the Shapiro–Wilk normality test. Normally distributed data were compared using unpaired two-tailed Student's *t*-test unless otherwise indicated. Data with unequal variance were compared using Welch's *t*-test. Non-normally distributed data were compared using the Mann–Whitney *U* test. $P<0.05$ was taken as statistically significant.

Results

In order to generate highly controllable and standardised data sets, we applied a fully defined feeder-free monolayer-based differentiation protocol to our hiPSC cultures (Fig. 1a), directing cardiac induction as previously described [39]. Spontaneous beating was regularly observed by day 8 (d8). Following differentiation, hiPSC-CM stained positive for cardiac marker alpha-actinin, with clear sarcomeric structures visible (Fig. 1b). 90.1 ± 1.6% of cells were alpha-actinin positive, indicating satisfactory differentiation efficiency (Fig. 1c). Following differentiation, hiPSC-CM were plated at low density (15,000/cm^{-2}) to ensure regular analysis of single, isolated cells which remain unaffected by electrical and paracrine influences of dense syncytial layers or cellular aggregates. Based on experimental and modelling data, cells assayed between d30 and d46 were designated as early-stage hiPSC-CM while d47–d80 were allocated to the late-stage development category. Cellular size was ascertained through longitudinal cross-sectional area measurement by tracing the perimeter of the hiPSC-CM using the freehand selection tool on ImageJ in a cohort of cells also utilised for patch-clamp experiments. Longitudinal cross-sectional area appeared unchanged in accordance with comparable membrane capacitance. The ratio between cellular area and capacitance indicated limited structural alterations in t-tubule density between early and late cultures (Fig. 1d). Isolated cells with no contact to neighbouring cells and clear membrane resolution were used for electrophysiological characterisation (Fig. 1e).

Increased systolic Ca^{2+} release from the SR of late hiPSC-CM cultures

Next, we assessed $I_{Ca,L}$-triggered Ca^{2+} transients (CaTs) at different stages of hiPSC-CM development. $I_{Ca,L}$ was initiated by a voltage-clamp protocol and was measured simultaneously with CaT (Fluo-3) in hiPSC-CM (Fig. 2a). Peak $I_{Ca,L}$ was significantly larger in late hiPSC-CM versus early culture (− 29.24 ± 3.98 vs. − 10.52 ± 1.27 pA/pF, *n*/*N* = 28/3 vs. 19/3, $P=0.0005$; Fig. 2b). Current–voltage relationships showed a positive shift in maximal current density in late cultures (Fig. 2c). Diastolic $[Ca^{2+}]_i$ was similar between both groups; however, systolic $[Ca^{2+}]_i$ was higher in late cultures. This was matched by a significant increase in CaT amplitude in late cells versus early cells (191.6 ± 26.81 vs. 134.3 ± 15.49 nmol/L, *n*/*N* = 28/3 vs. 19/3, $P=0.0358$; Fig. 2d). The $Ca_v1.2$ blocker nifedipine (1 µmol/L) produced a reduction in $I_{Ca,L}$ in every instance, suggesting presence of

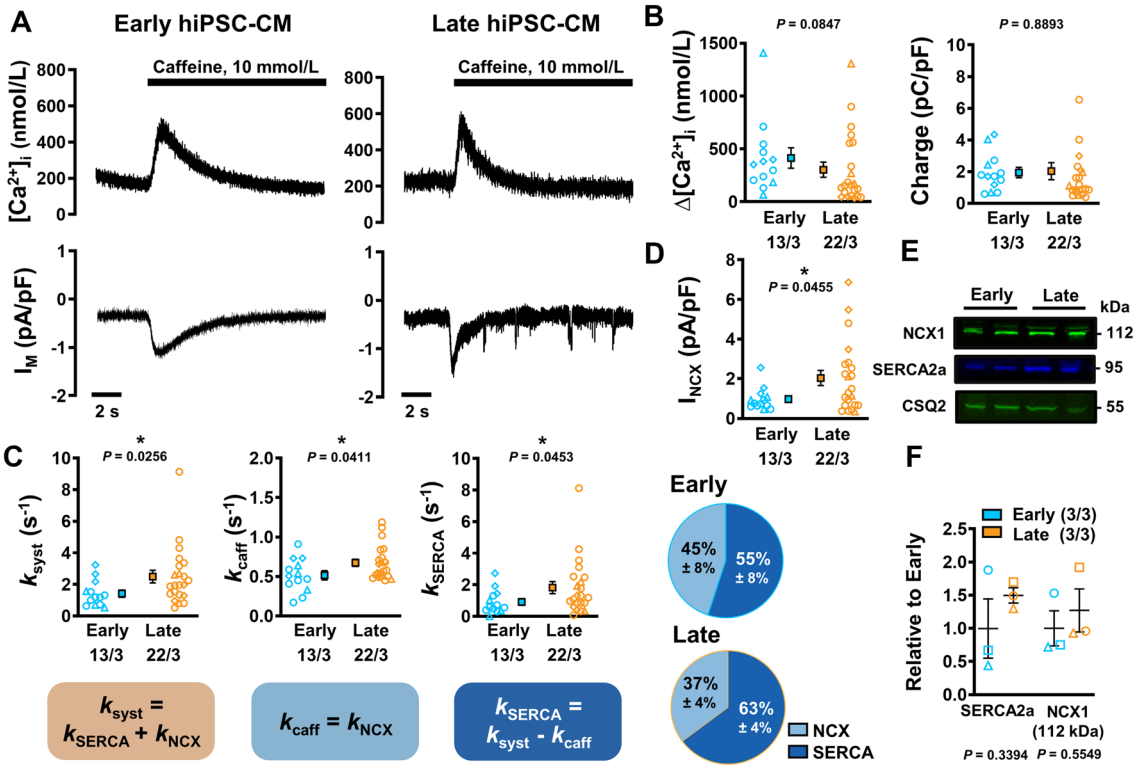

Fig. 3 Caffeine-induced Ca^{2+} transients (cCaT) with corresponding transient-inward currents (I_{NCX}) to assess sarcoplasmic reticulum (SR) Ca^{2+} content in isolated early and late human induced pluripotent stem cell-derived cardiomyocytes (hiPSC-CM). **A** Representative cCaT (upper) and corresponding I_{NCX} (lower) in early (left) and late hiPSC-CM (right). **B** SR Ca^{2+} load, quantified as cCaT amplitude (left), or integrated membrane current (Charge; right). **C** Rate constants of Ca^{2+} transport k_{syst} (far left), k_{caff} (centre left), k_{SERCA} (calculated as the difference between k_{syst} and k_{caff}; centre right) and the resulting relative proportions of NCX and SERCA-mediated cytosolic Ca^{2+} removal in early and late hiPSC-CM (far right). **D** Peak I_{NCX}. **E** Representative western blots showing the expression of NCX1 and SERCA2a against CSQ2. **F** Quantification of NCX1 and SERCA2a expression relative to early hiPSC-CM (3 independent experiments per group). Data are mean ± SEM. *$P < 0.05$ versus early hiPSC-CM culture by Welch's t test or Mann–Whitney *U* test (B). Symbols represent separate differentiations. *n/N* = number of hiPSC-CM/differentiation

functional $Ca_V1.2$ from an early stage in cellular differentiation (Online Fig. S1).

SR Ca^{2+} content was assessed through caffeine application (10 mmol/L) after cessation of the $I_{Ca,L}$-activating protocol (Fig. 3a). The resulting caffeine-induced CaT (cCaT) amplitude and integral of corresponding membrane current (reflecting NCX-mediated Ca^{2+} extrusion; charge) were comparable between late and early hiPSC-CM cultures, indicating that higher CaT amplitude in late cells is mainly due to increased trigger $I_{Ca,L}$ (Fig. 3b).

Altered diastolic Ca^{2+}-handling in late hiPSC-CM cultures

Diastolic Ca^{2+} removal from the cytosol was faster in late cultures versus early cultures as indicated by the rate constant of systolic CaT decay (inverse of CaT τ, k_{syst}, Fig. 3c). Decay of cCaT mainly reflects NCX-mediated Ca^{2+} removal and was also faster in more mature cells. This is consistent with higher peak I_{NCX} density (2.03 ± 0.38 vs. 0.97 ± 0.16 pA/pF, *n/N* = 22/3 vs. 13/3, $P = 0.0455$; Fig. 3d), pointing to increased NCX activity in late hiPSC-CM cultures. In accordance, average protein expression of NCX1 was numerically larger in late hiPSC-CM (Fig. 3e, f). Absolute levels of housekeeping protein calsequestrin (CSQ2) showed no difference between early and late cultures (1.00 ± 0.33 vs. 1.03 ± 0.28 a.u relative to early, *n/N* = 3/3 vs. 3/3 [not shown]). The rate constant k_{SERCA} represents the difference between the rate constant of cCaT decay and that of systolic CaT decay [15]. k_{SERCA} was significantly larger in late cultures versus early cultures (1.82 ± 0.38 vs. 0.91 ± 0.21 s^{-1}, *n/N* = 22/3 vs. 13/3, $P = 0.0453$; Fig. 3c). This was supplemented by the western blot findings (Fig. 3e, f).

Confocal line-scan analysis of Ca^{2+} sparks revealed a tendency towards decreased Ca^{2+} spark frequency and significantly decreased Ca^{2+} leak from the SR in late hiPSC-CM cultures versus early (12.73 ± 5.06 vs. 30.35 ± 9.04 100 μm^{-1} s^{-1}, *n/N* = 41/7 vs. 39/2, $P = 0.0416$; Online

Fig. S2). In addition, spontaneous beating rate, a marker of automaticity, was decreased in late-stage hiPSC-CM (0.45 ± 0.18 vs. 0.79 ± 0.4 Hz, $n/N = 11/2$ vs. 12/2, $P = 0.0067$; Online Fig. S2).

Maturation dependent increase of peak I_{Na} during long-term culture

Peak I_{Na} was significantly larger in late-stage hiPSC-CM (−71.12 ± 15.77 vs. −26.63 ± 4.89 pA/pF, $n/N = 29/3$ vs. 21/3; $P = 0.0237$) with current–voltage relationships showing a slight negative shift in peak current density (Fig. 4a, b). $I_{Na,L}$ was subsequently measured as current responsive to tetrodotoxin (TTX, 10 µmol/L) in both late and early hiPSC-CM cultures (Fig. 4c). In contrast to peak I_{Na}, integrated $I_{Na,L}$ was not different between early and late hiPSC-CM (Fig. 4d).

Emergence of robust I_{K1} during long-term culture

K^+ currents are responsible for repolarisation and stabilisation of resting membrane potential (RMP). Assessment of the rapid component of the delayed rectifier K^+ current (I_{Kr}) following complete block with 25 µmol/L E-4031 revealed no age-dependent difference in tail current between late and early hiPSC-CM (−2.94.12 ± 0.55 vs. −3.84 ± 0.82 pA/pF, $n/N = 77/4$ vs. 60/4, $P = 0.6733$; Fig. 5a, b). Comparable I–V curves and pharmacology were also observed across early and late hiPSC-CM (Online Fig. S3).

The basal inward-rectifier K^+ current I_{K1} was measured in both early- and late-stage hiPSC-CMs using a modified ramp protocol with high extracellular [K^+] (20 mmol/L), which produces a positive shift in reversal potential and allows for precise current detection, as previously described [76] (Fig. 5c). Ba^{2+}-sensitive I_{K1} was markedly increased in late-stage cells compared with early cells in both inward direction (− 100 mV: −48 ± 12.3 vs. −12.63 ± 2.28 pA/pF, $n/N = 17/4$ vs. 43/6, $P = 0.0004$; Fig. 5c, d) and outward direction (− 10 mV: 4.10 ± 0.62 vs. 2.75 ± 0.47 pA/pF, $n/N = 17/4$ vs. 43/6, $P = 0.009$), without changes in rectification (Online Fig. S4). In accordance, expression of Kir2.1 protein was significantly increased in late hiPSC-CM cultures (Fig. 5e, f).

Computational modelling of hiPSC-CM Ca^{2+}-handling maturation

We employed computational modelling to assess (1) whether the experimentally identified changes in $I_{Ca,L}$, I_{NCX} and SERCA are sufficient for the observed changes in hiPSC-CM Ca^{2+}-handling and (2) to predict the maturation-dependent changes in AP characteristics resulting from the remodelling of all ionic currents. The recent Kernik et al. hiPSC-CM model was fit to our experimental data from early- or late-stage hiPSC-CM [36]. Besides the changes in $I_{Ca,L}$, I_{NCX} and SERCA function, adjustments in Ca^{2+} buffering and background Ca^{2+} influx were needed to reproduce the experimentally observed Ca^{2+}-handling properties (Online Table S2).

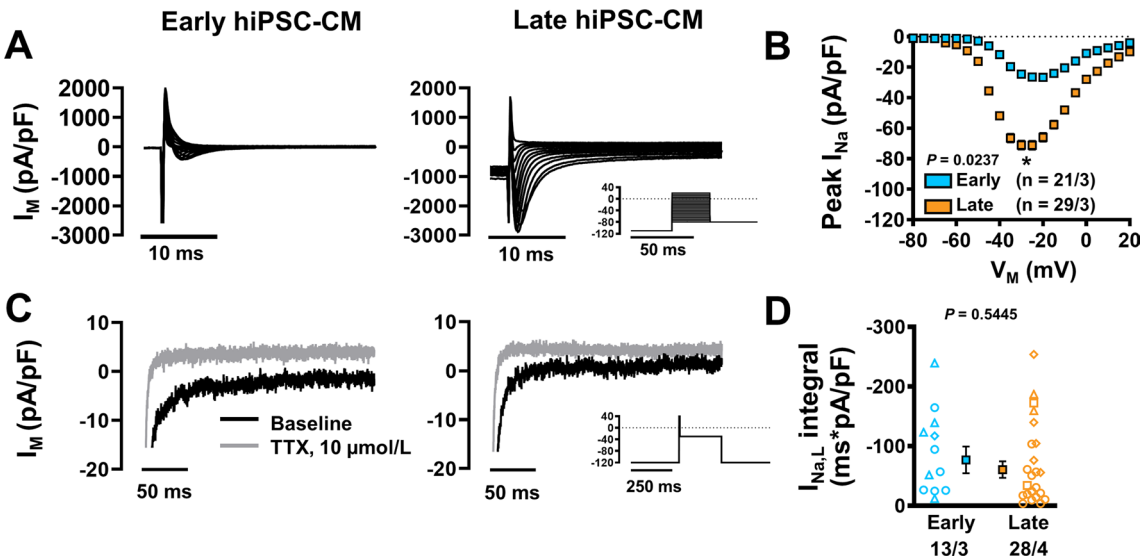

Fig. 4 Peak Na^+ current (I_{Na}) and late Na^+ current ($I_{Na,L}$) in isolated early and late human induced pluripotent stem cell-derived cardiomyocytes (hiPSC-CM). **A** Representative I_{Na} in early (left) and late hiPSC-CM (right). Inset: voltage-clamp protocol. **B** Current–voltage relationship for I_{Na}. **C** Representative $I_{Na,L}$ in early (left) and late hiPSC-CM (right) in the absence (Baseline) or presence of 10 µmol/L tetrodotoxin (TTX). Inset: modified voltage-clamp protocol to accentuate late current (as described in Poulet et al. [56]). **D** $I_{Na,L}$ integral. Data are mean ± SEM. $^*P < 0.05$ versus early hiPSC-CM culture. Symbols represent separate differentiations. n/N = number of hiPSC-CM/differentiation

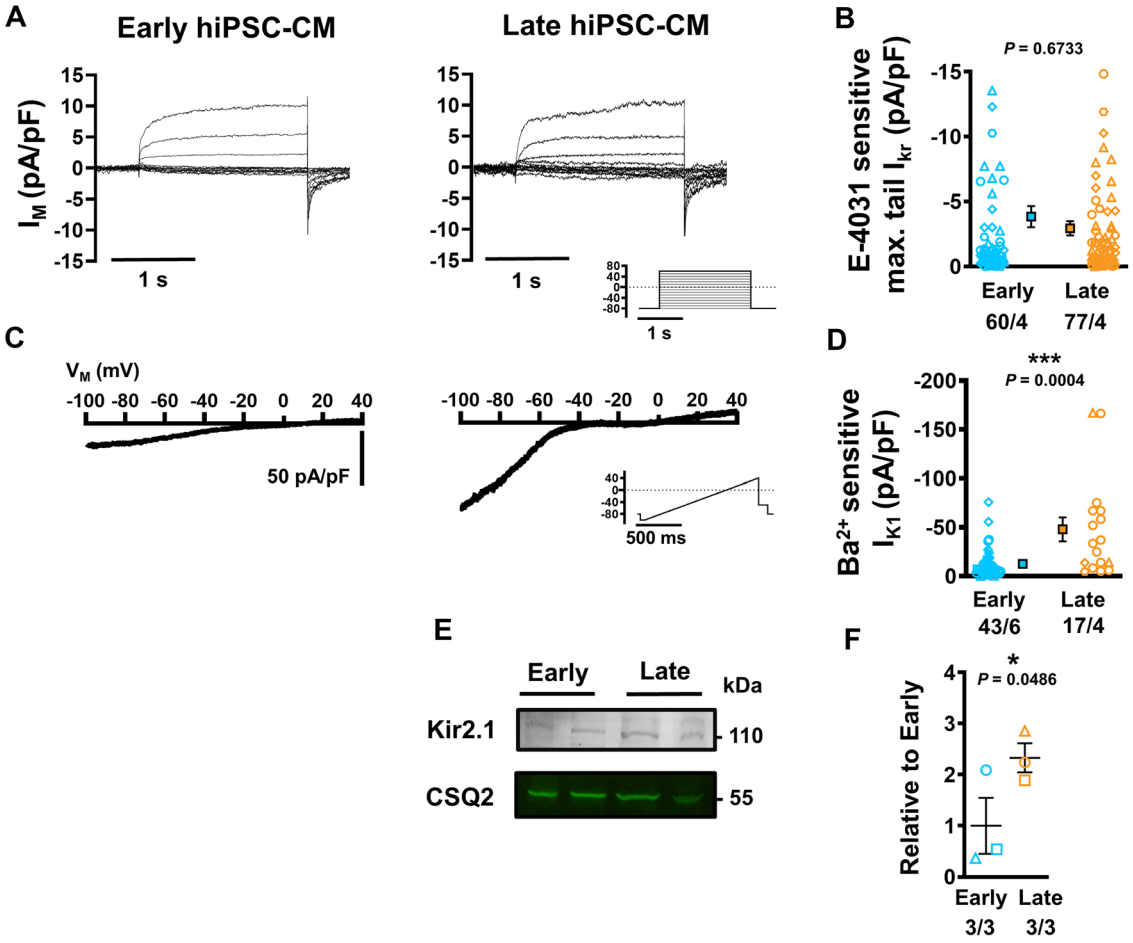

Fig. 5 Rapid component of the delayed-rectifier K^+ current (I_{Kr}) and basal inward-rectifier K^+ current (I_{K1}) in isolated early and late human induced pluripotent stem cell-derived cardiomyocytes (hiPSC-CM). **A** Representative I_{Kr} in early (left) and late hiPSC-CM (right). Inset: voltage-clamp protocol. **B** Maximum tail I_{Kr} defined as E4031-sensitive current. **C** Representative recordings of I_{K1} in early (left) and late hiPSC-CM (right) during a depolarising ramp pulse protocol (inset). **D** Peak I_{K1} defined as Ba^{2+}-sensitive current. **E** Representative western blots showing the expression of Kir2.1 against CSQ2 (same gel as Fig. 3). **F** Quantification of Kir2.1 expression relative to early hiPSC-CM (3 independent experiments per group). Data are mean ± SEM. $*P<0.05$ $***P<0.001$ versus early hiPSC-CM culture. Symbols represent separate differentiations. n/N = number of hiPSC-CM/differentiation

Nevertheless, with this limited number of changes, the model was able to reproduce all experimentally observed properties of early- and late-stage hiPSC-CM (Online Figs. S4–S8). Of note, interpolation of these Ca^{2+}-handling parameters produced non-linear maturation-dependent changes in CaT properties that reflected the non-linear patterns observed in the experimental data (Fig. 6a). These modelling data suggest that gradual increases or decreases in expression levels of Ca^{2+}-handling proteins may produce complex temporal changes at the cellular level.

Identification and experimental corroboration of AP shortening during long-term culture

Under current-clamp conditions at 0.5 Hz, the in silico hiPSC-CM model predicted a maturation-dependent decrease in action potential duration (APD) from 365 ms at d30 to 174 ms at d70. (Fig. 6b). In order to corroborate and validate the maturation-dependent AP shortening predicted by the modelling data, APs were measured at multiple time points during long-term hiPSC-CM monolayer culture (Fig. 6c). Under experimental current-clamp conditions, hiPSC-CM indeed displayed maturation-dependent changes, with late cells showing APD shortening at 50% and 90% repolarisation (APD_{50}, APD_{90}) compared with early-stage cells (APD_{50}: 163 ± 35.76 vs. 205.34 ± 26.87 ms [not shown]; APD_{90}: 259.1 ± 42.13 vs. 393.8 ± 38.65 ms, n/N = 13/3 vs. 23/3, $P = 0.0358$; Fig. 6d). Repolarisation fraction ([APD_{90}-APD_{50}]/APD_{90}), a representation of repolarisation profile and, therefore, an index of cardiomyocyte subtype, remained unchanged throughout hiPSC-CM culture suggesting the absence of a

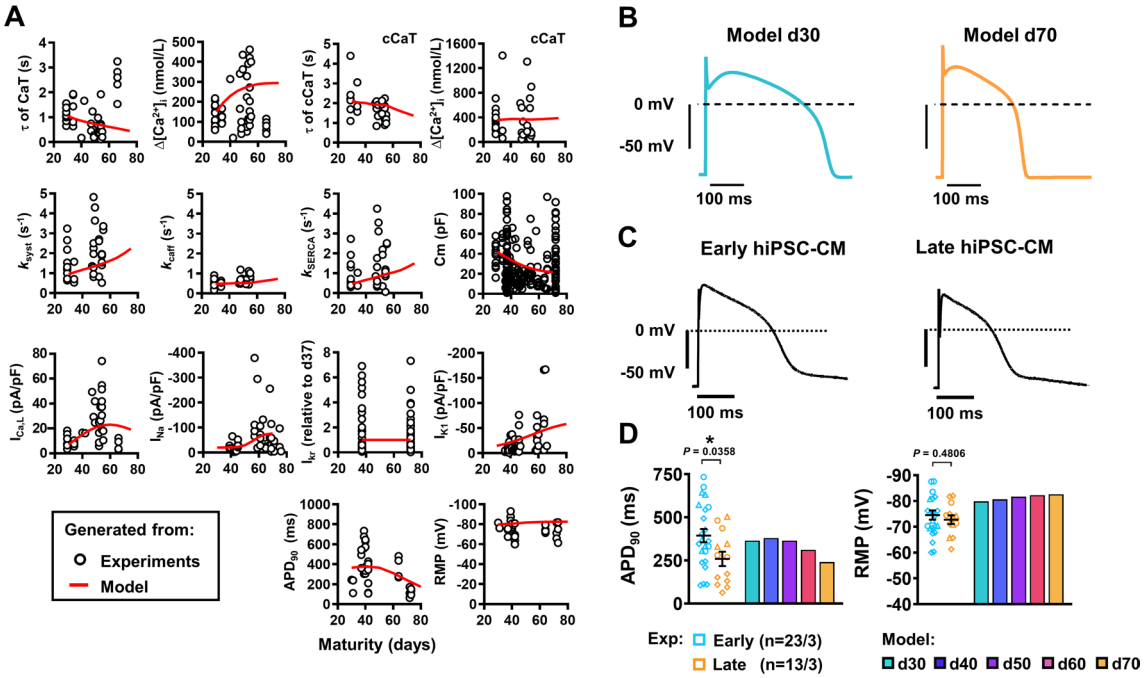

Fig. 6 Overview of maturation-dependent changes in cellular Ca^{2+} dynamics and electrophysiology which drive action potential (AP) characteristics in experimental and in silico human induced pluripotent stem cell-derived cardiomyocytes (hiPSC-CM). **A** Plots of the experimental data for all measured electrophysiological cellular parameters in aging hiPSC-CM. The red line indicates the in silico output of expected results demonstrating non-linear maturation-dependent characteristics. **B** Simulated steady-state AP traces at 0.5 Hz in d30 and d70 modelled hiPSC-CM. The stimulus current (I_{stim}) was set to − 120 µA/µF and the hyperpolarising current (I_{hyper}) was set to 0.2 µA/µF. **C** Representative experimental AP traces in early (left) and late hiPSC-CM (right). **D** Comparison of experimental and model AP properties during 0.5 Hz pacing: resting membrane potential (RMP; left) and AP duration at 90% repolarisation (APD_{90}; right). Experimental data are mean ± SEM. $^*P < 0.05$. Symbols represent separate differentiations. *n*/*N* = number of hiPSC-CM/differentiation

transient subtype shift during long culture periods (Online Fig. S9). Upstroke velocity and AP amplitude (APA) were increased in late-stage hiPSC-CM (upstroke velocity: 66.98 ± 20.9 vs. 30.22 ± 10.24 mV/ms, $n = 10/3$ vs. 16/3, $P = 0.0309$; APA: 123.7 ± 4.06 vs. 110.6 ± 3.67 mV, $n = 13/3$ vs. 23/3, $P = 0.0298$; Online Fig. S9), consistent with the increase in I_{Na}. No change was observed between early- or late-stage RMP both in the presence (Fig. 6d) and absence of injected current (Online Fig. S9), which is in line with our in silico simulations. In silico, the unchanged RMP could be attributed to a parallel increase in depolarizing NCX during maturation, counterbalancing the effects of increased I_{K1} on RMP.

We then went back to the model to establish the major ionic determinant of the AP shortening by making use of the perfect control offered by in silico models. Preventing the maturation-dependent increase in I_{K1} abolished the APD reduction and eventually elicited spontaneous activity (Fig. 7a). A progressive depolarisation of RMP was also observed due to increased NCX (Fig. 7a, b), highlighting the importance of maturation-dependent changes in I_{K1} for cellular electrophysiology of hiPSC-CM. To further highlight the electrophysiological consequence of increased I_{K1} in hiPSC-CM experimentally, we evaluated the effects of partial I_{K1} inhibition. Older cells showed a 50% increase in AP duration following I_{K1} blockade with $BaCl_2$ (1 mmol/L) compared to a non-significant 5% change in early cells (Online Fig. S10). In addition, application of $BaCl_2$ produced more instability and a high occurrence of arrhythmogenic events in late cells compared to early hiPSC-CM (Online Fig. S10).

Discussion

In this multimodal study, we have identified dynamic developmental behaviour of key ionic currents and Ca^{2+}-handling properties in hiPSC-CM during long-term culture. Older hiPSC-CM display significantly larger $I_{Ca,L}$ density along with temporally complex SERCA and NCX development (Figs. 2, 3). I_{Na} and I_{K1} densities were also significantly increased in late-stage cells, which increases AP upstroke velocity and shortens APD, respectively (Figs. 4, 5, 6; Online Fig. S9). In addition, we updated an existing in silico hiPSC-CM model which reproduced our experimental findings. Interpolation of the model parameters as a function of

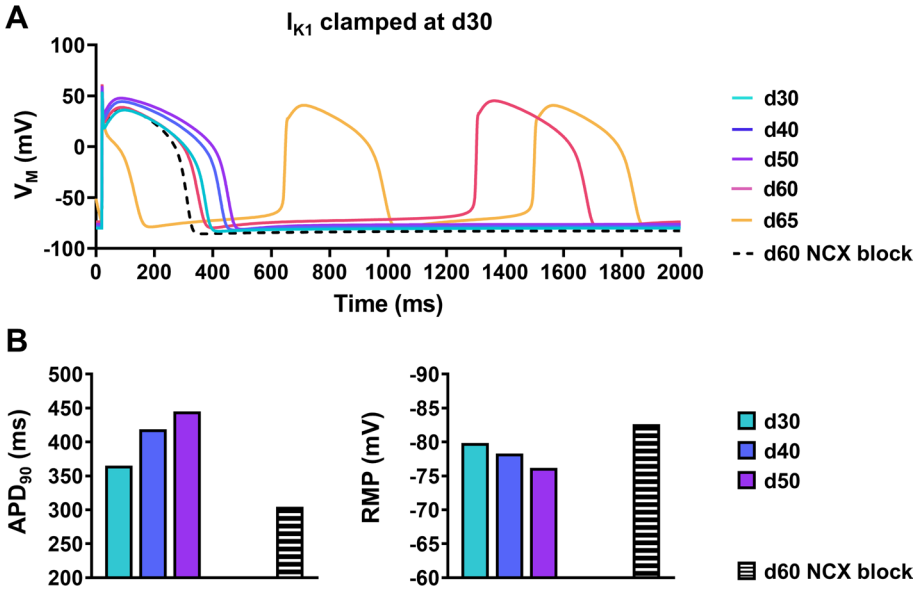

Fig. 7 The role of inward-rectifier K^+ current (I_{K1}) and inward Na^+/Ca^{2+}-exchanger (NCX) current in maturity-dependent action potential (AP) shortening in in silico human induced pluripotent stem cell-derived cardiomyocytes (hiPSC-CM). **A** Steady-state AP simulations over increasing ages with I_{K1} clamped at 30 days of maturation (solid lines), as well as during acute inhibition of NCX at d60 (dashed line). Note: automaticity is observed at d60 and d65. The stimulated AP at d65 is short due to the incomplete repolarisation of the preceding spontaneous AP. **B** AP duration at 90% repolarisation (APD_{90}; left) and resting membrane potential (RMP; right) at increasing stages of development in the absence of I_{K1} maturation, as well as at d60 with acute NCX inhibition (black/white bars). Note: RMP and APD_{90} values for d60 and d65 in the absence of NCX inhibition are not shown due to abnormal automaticity

cellular age revealed complex, nonlinear temporal dynamics of hiPSC-CM electrophysiological development that was consistent with our experimental data (Fig. 6a). Using this tool, we also established the primary ionic determinant of APD shortening by abolishing the maturation-dependent increase in I_{K1}, which successfully attenuated APD reduction (Fig. 7). Finally, we have developed an open-source user interface which allows for multi-level simulations of cellular electrophysiology and Ca^{2+}-handling across a wide range of cellular ages post differentiation (Fig. 8). This tool also exhibits the capacity for age-based deductions of drug-induced proarrhythmic risk.

In this study, cardiomyocyte maturity is defined as a general phenotypical state equivalent to that of a fully developed native adult ventricular cardiomyocyte. In particular, this study assesses time-dependent changes in hiPSC-CM calcium handling and electrophysiology as key components of their maturation state. Similar to previous work, our hiPSC-CM show functional variability and an immature electrical phenotype characterized by less negative RMP, slower AP upstroke velocity and automaticity [12, 23, 34]. This is not surprising, as native adult cardiomyocytes develop continually within a complex and precisely organised system over a lifetime of phasic load and physiological stimulation in vivo.

Maturation of cytosolic Ca^{2+} homeostasis

There is a paucity of systematic studies assessing passive maturation of electrophysiological and Ca^{2+}-handling processes in isolated hiPSC-CM cultured for more than 30 days after differentiation onset. Here, we report evidence of robust Ca^{2+}-handling and operational SR Ca^{2+} stores in early hiPSC-CM, similar to results reported by Hwang et al. [27]. However, as our cells aged further, they displayed increased $I_{Ca,L}$ and CaT amplitude (Fig. 2) along with a functional increase in key Ca^{2+}-removal mechanisms, NCX and SERCA (Fig. 3). The present work expands on that of Hwang et al. and indicates that further maturation of Ca^{2+}-handling machinery is possible in hiPSC-CM under prolonged culture of more than 50 days. Previous studies using cells under 30 days of age have outlined a dominant role of NCX function and poor SR development in hiPSC-CM [44]. Increased NCX-mediated electrogenic activity coupled with a leaky SR leads to increased incidence of delayed after-depolarisations (DADs) and could play a role in the cellular automaticity typically displayed by hiPSC-CM. The interplay of low inward-rectifier K^+ current density paired with increased funny current (I_f) is assumed to be the major cause of spontaneous activity in hiPSC-CMs [66]. However, previous studies have shown that I_f density alone is not sufficient to induce automaticity in hESC-CM. Instead, Ca^{2+} release from the SR has been hypothesised as a major

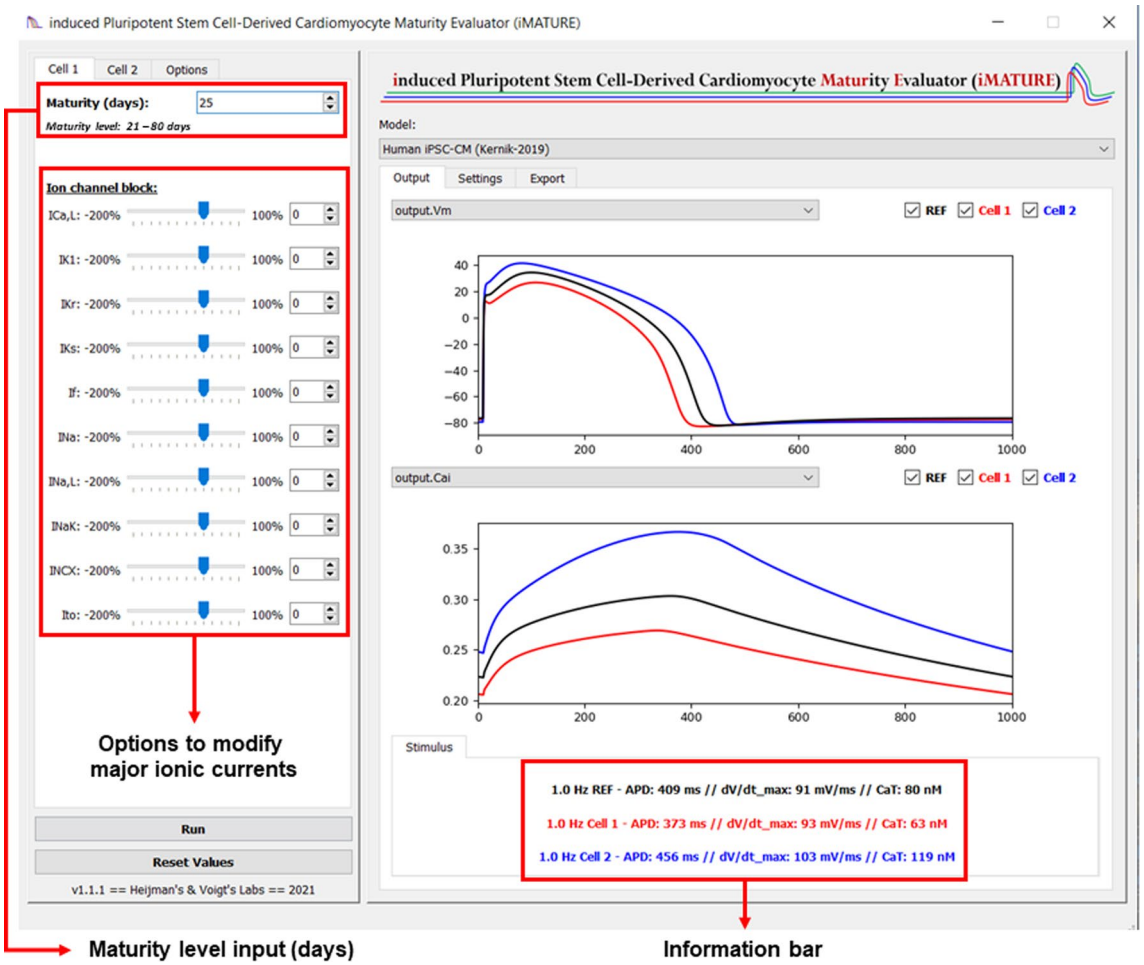

Fig. 8 Screenshot of the induced pluripotent stem cell-derived cardiomyocyte maturity evaluator (iMATURE) software tool. The iMATURE tool incorporates the experimentally-observed maturity-dependent changes on cardiac ion channels (i.e., I_{Na}, I_{NaL}, $I_{Ca,L}$, I_{Kr} and I_{K1}) and Ca^{2+}-handling proteins in the Kernik hiPSC-CM model [36]. The tool enables the simulation and comparison of two maturity levels simultaneously under different experimental conditions. It also enables rapid evaluation of the effects of inhibition of major ionic currents

driver of automaticity with RyR2 abolition leading to cellular quiescence [38]. I_{K1} also influences cellular automaticity and previous work highlights a potential regulatory effect of increased cytosolic Ca^{2+} flux during diastole by increasing rectification in cardiomyocytes, effectively blocking I_{K1} and facilitating spontaneous beating [16, 80]. We, among others, report high SR Ca^{2+} leak and increased automaticity in early hiPSC-CM. However, as the cells age, we noted a lower incidence of Ca^{2+} sparks and decreased SR Ca^{2+} leak coupled with a significant decrease in spontaneous beating rate (Online Fig. S2). Interestingly, SR Ca^{2+} load remained comparable between early and late cultures, suggesting coordinated development of Ca^{2+}-handling machinery during maturation (Fig. 3). The increased NCX function identified in older hiPSC-CM was not strongly replicated at the protein level, possibly also implicating the concurrent development of intracellular signalling, trafficking and phosphorylation mechanisms. Indeed, increased cAMP and cGMP have been found to enhance forward mode NCX function through protein kinase activation in older, but not in younger, embryonic mouse ventricular cardiomyocytes [58].

Together, these data point to a strong age-dependence of SR function under standardised and prolonged culture conditions. When interpolated in silico, a non-linear behaviour with exponential consolidation of SERCA activity is observed as hiPSC-CM age over time (Fig. 6). Our in silico model is the first to incorporate a detailed analysis of CaT and Ca^{2+}-reuptake mechanisms across various stages of hiPSC-CM maturation.

Table 1 Comparison of electrophysiological properties of human induced pluripotent stem-cell derived cardiomyocytes

	This study, "Early"	This study, "Late"	Zhao et al. [81]	Zhao et al. [81]	Ma et al. [50]	Lee et al. [43]
Capacitance (pF)	43	31	22–25	22–25	16	
I_{Na}						
Peak I_{Na} density	− 27	− 71	− 30	− 53	− 217	− 163
Potential	− 25	− 25	− 40	− 40	− 20	− 60
$[Na]_e$ for Peak I_{Na} (mM)	5	5	10	10	10	5
$[Na]_e$ for Peak I_{Na} (mM)	5	5	20	20	50	50
Temperature (°C)	37	37	20	20	36	37
E_{rev} (mV)	0	0	18	18	43	62
Conductance (S/F)	1065	2845	522	918	3447	1343
$I_{Ca,L}$						
$I_{Ca,L}$ density	− 11	− 29	− 10	− 13	− 17	− 7
Temperature (°C)	37	37	22–25	22–25	22–25	37
I_{K1}						
I_{K1} density (pA/pF)	− 13	− 48	− 1	− 2	− 2	− 5
Step potential	− 100	− 100	− 120	− 120	− 123	− 150
$[K]_i$ for I_{K1} (mM)	150	150	126	126	150	140
$[K]_e$ for I_{K1} (mM)	20	20	6	6	5	5
Temperature (°C)	37	37	20	20	37	37
E_{rev} (mV)	− 54	− 54	− 77	− 77	− 89	− 87
Conductance (S/F)	274	1040	16	45	67	81
I_{Kr}						
I_{Kr} tail (pA/pF)	− 4	− 3				
I_{Kr} step (pA/pF)			1	1	0.4	2
Temperature (°C)	20	20	20	20	37	37
Action Potential						
RMP (mV)	− 75	− 73	− 80	− 80	− 76	− 66
dV/dt_{max} (V/s)	30	67	125	130	28	45
APA (mV)	110	123	140	140	104	108
APD_{90} (ms)	394	259	290	300	415	492
Frequency	0.5	0.5	1	1	Spontaneous	Spontaneous
Temperature (°C)	37	37	20	20	37	37
Days after differentiation onset	30–46	47–80	30–40	50–60	10–21*	7–28*

Table 1 (continued)

	Veerman et al. [71]**	Herron et al. [23]	Sala et al. [63]	Doss et al. [12]	Lemoine et al. [46]	Horváth et al. [25]
Capacitance (pF)					28	31
I_{Na}						
Peak I_{Na} density	− 94	− 105			− 10	
Potential	− 20	− 30			− 30	
$[Na]_i$ for Peak I_{Na} (mM)	3	5			5	
$[Na]_e$ for Peak I_{Na} (mM)	20	20			5	
Temperature (°C)	20	20			20	
E_{rev} (mV)	48	35			0	
Conductance (S/F)	1378	1615			343	
$I_{Ca,L}$						
$I_{Ca,L}$ density	− 50		− 9			
Temperature (°C)	36		37			
I_{K1}						
I_{K1} density (pA/pF)		− 6		− 3		− 33
Step potential		− 120		− 100		− 100
$[K]_i$ for I_{K1} (mM)		148		120		150
$[K]_e$ for I_{K1} (mM)		5		5		20
Temperature (°C)		20		36		37
E_{rev} (mV)		− 84		− 83		− 54
Conductance (S/F)		173		201		717
I_{Kr}						
I_{Kr} tail (pA/pF)			2	1		
I_{Kr} step (pA/pF)						
Temperature (°C)			37	37		
Action Potential						
RMP (mV)	− 80**	− 71	− 48	− 66		
dV/dt_{max} (V/s)	230	147		24		
APA (mV)	120	116	90	103		
APD_{90} (ms)	160	NA	135	325		
Frequency	1		1	Spontaneous		
Temperature (°C)	37	37	37	37		
Days after differentiation onset	39–44	4–7*	20–30	35–74	42	42

Currents are dependent on ion concentrations, which differ between studies. Be cautious with direct comparisons which should ideally be made between groups studies under identical conditions

*Days post thaw

**Dynamic clamp

Table 2 Electrophysiological properties of hiPSC-CM in engineered heart muscle

	Lemoine et al. [46]	Lemoine et al. [45]	Horváth et al. [25]	Tiburcy et al. [68]
Capacitance (pF)	28		47	
I_{Na}				
Peak I_{Na} density	− 19			
Potential	− 30			
$[Na]_i$ for Peak I_{Na} (mM)	5			
$[Na]_e$ for Peak I_{Na} (mM)	5			
Temperature (°C)	20			
E_{rev} (mV)	0			
Conductance(S/F)	633			
$I_{Ca,L}$				
$I_{Ca,L}$ density				
Temperature (°C)				
I_{K1}				
I_{K1} density (pA/pF)			− 14	
Step potential			− 100	
$[K]_i$ for I_{K1} (mM)			150	
$[K]_e$ for I_{K1} (mM)			20	
Temperature (°C)			20	
E_{rev} (mV)			− 51	
Conductance (S/F)			285	
I_{Kr}				
I_{Kr} tail (pA/pF)				
I_{Kr} step (pA/pF)				
Temperature (°C)				
Action Potential				
RMP (mV)	− 78	− 78	− 75	− 72
dV/dt_{max} (V/s)	219	348		107
APA (mV)	103	109		97
APD_{90} (ms)	NA	255	271	436
Frequency (Hz)	1	1	1	Spontaneous
Temperature (°C)	37	37	37	37
Days after differentiation onset	42	39–114	42	NA

Currents are dependent on ion concentrations, which differ between studies. Be cautious with direct comparisons which should ideally be made between groups studies under identical conditions

Maturation of cellular electrophysiology

An overview of hiPSC-CM electrophysiology from 2D and 3D preparations compared with our data and with data from native ventricular cardiomyocytes is provided in Tables 1, 2 and 3. It is important to emphasize that ion currents are dependent on experimental ion concentrations, which differ between studies. Direct comparisons should, therefore, be made with caution, ideally between groups studied under identical conditions. Nevertheless, similar to previous studies, our hiPSC-CM show a relatively immature phenotype characterized by less negative RMP, slower AP upstroke velocity and automaticity [8, 18, 26]. Lack of I_{K1} is a hallmark of hiPSC-CM [23, 50]. To allow for comparison between studies performed at different extracellular K^+ concentrations and temperatures, we estimated the conductance values based on reported I_{K1} densities and calculated the resulting reversal potentials (E_{rev}, Tables 1, 2 3). The reduced I_{K1} conductance observed throughout all studies is a major contributor to the less negative RMP and thereby facilitates the occurrence of spontaneous activity in hiPSC-CM constructs [24, 31, 34]. In addition, the depolarized RMP also causes reduced availability of voltage-dependent Na^+ channels due to incomplete recovery from inactivation. Therefore, the reduced I_{K1} may also contribute to the typically lower AP upstroke velocity in hiPSC-CM [12, 43, 50]. This

Table 3 Electrophysiological properties of native human ventricular cardiomyocytes

	Sakakibara et al. [61]	Valdivia et al. [69]	Magyar et al. [51]**	Mewes et al. [53]	Konarzewska et al. [41]	Koumi et al. [42]*
Capacitance (pF)	194	168		189	96	
I_{Na}						
Peak I_{Na} density	− 20	− 49				
Potential	− 40	− 40				
$[Na]_i$ for Peak I_{Na} (mM)	5	1				
$[Na]_e$ for Peak I_{Na} (mM)	5	5				
Temperature (°C)	17	20				
E_{rev} (mV)	0	41				
Conductance (S/F)	505	608				
$I_{Ca,L}$						
$I_{Ca,L}$ density			10	4		
Temperature (°C)			37	21–23		
I_{K1}						
I_{K1} density (pA/pF)			− 4		− 18	− 30
Step potential			− 100		− 140	− 120
$[K]_i$ for I_{K1} (mM)			120		525	141
$[K]_e$ for I_{K1} (mM)			5		4	5
Temperature (°C)			37		20	37
E_{rev} (mV)			− 83		− 123	− 87
Conductance (S/F)			210		1083	914
I_{Kr}						
I_{Kr} tail (pA/pF)			0			
I_{Kr} step (pA/pF)						
Temperature (°C)			37			
Action Potential						
RMP (mV)			− 82			
dV/dt_{max} (V/s)			215			
APA (mV)			107			
APD_{90} (ms)			213			395
Frequency			1			1
Temperature (°C)			37			37
Heart failure patients (+/−)	+	−	−	−	−	−

Table 3 (continued)

	Bailly et al. [2]	Iost et al. [28]	Hartmann et al. [20]*	Lemoine et al. [46]**	Lemoine et al. [45]**
Capacitance (pF)					
I_{Na}					
Peak I_{Na} density					
Potential					
$[Na]_i$ for Peak I_{Na} (mM)					
$[Na]_e$ for Peak I_{Na} (mM)					
Temperature (°C)					
E_{rev} (mV)					
Conductance (S/F)					
$I_{Ca,L}$					
$I_{Ca,L}$ density					
Temperature (°C)					
I_{K1}					
I_{K1} density (pA/pF)	− 60				
Step potential	− 170				
$[K]_i$ for I_{K1} (mM)	120				
$[K]_e$ for I_{K1} (mM)	4				
Temperature (°C)	20				
E_{rev} (mV)	− 86				
Conductance (S/F)	714				
I_{Kr}					
I_{Kr} tail (pA/pF)		0.3			
I_{Kr} step (pA/pF)					
Temperature (°C)		37			
Action Potential					
RMP (mV)			− 80	− 75	− 78
dV/dt_{max} (V/s)			182	253	176
APA (mV)			130	105	111
APD_{90} (ms)			553	NA	397
Frequency			1	1	1
Temperature (°C)			37	37	37
Heart failure patients (+/−)	−	−	+	+	+

Currents are dependent on ion concentrations, which differ between studies. Be cautious with direct comparisons which should ideally be made between groups studies under identical conditions

*Action potentials from isolated cardiomyocytes

**Action potentials from intact tissue preparations

combination induces proarrhythmic traits in hiPSC-CM which presents a severe disadvantage for their use for drug safety screening initiatives such as CiPA. Targeting I_{K1} is therefore an important aspect of enhancing hiPSC-CM maturity and several methods exist to increase inward rectifier density. The hybrid method of dynamic patch clamp aims to overcome this limitation using an in silico ion channel model to adjust hyperpolarising current injection in real time based on the measured membrane potential [18, 52]. This technology is promising; however, it cannot capture native regulation of I_{K1}, e.g., by intracellular Ca^{2+} or Na^{+} [22, 75, 80]. Our combination of standardised serum-free differentiation and prolonged monolayer culture of > 50 days is sufficient to produce a 70% increase in I_{K1} density with increased I_{Na} and concomitant increases in AP upstroke velocity (Figs. 4, 5, Online Fig. S9). Similar maturation-dependent increases in I_{K1} density have been reported previously in hESC-CMs during prolonged culture [37, 64]. Doss et al. reported a transient increase in I_{K1} density in hiPSC-CMs after 2 months, followed by a decrease after 4 months [12]. Our in silico extrapolation of I_{K1} maturation does not support this parabolic developmental pattern, which could be due to differences in cellular culture techniques or their harsher dissociation procedures prior to measurement.

In the majority of studies, the maximal peak I_{Na} amplitude appears to be larger in hiPSC-CM compared with native cardiac tissue (Tables 1, 2, 3). This contradicts the lower expression levels of the underlying Nav1.5 subunit which are found in hiPSC-CM in comparison to human native ventricular cardiomyocytes [7]. Furthermore, direct comparison of peak I_{Na} currents is often hindered by different experimental conditions such as extracellular Na^{+} concentration and temperature. A direct comparison of hiPSC-CM and native human ventricular cardiomyocytes by Lemoine et al. suggests that peak I_{Na} currents are indeed lower in hiPSC-CM [46]. In addition, Lemoine et al. provide evidence for higher peak I_{Na} currents in more advanced 3D tissue culture models. This is in agreement with our study and a previous study in hiPSC-CM showing a tendency towards increased peak Na^{+} current in older hiPSC-CM [81]. Taken together, it appears that electrophysiological maturation of hiPSC-CM is associated with increased I_{Na} densities, although AP upstroke velocity remains low compared to adult ventricular cardiomyocytes.

The present work identifies maturation-dependent I_{K1} augmentation as a key mediator of AP shortening in hiPSC-CM. Rapid delayed rectifier K^{+} currents remained unchanged throughout long term culture (Fig. 5) and, in the absence of maturation-dependent changes of I_{K1} in silico, APD prolonged as the cells matured in the presence of increasing cytosolic Ca^{2+} activity (Fig. 7). This is in contrast to the Paci model [54], which attributes maturation-dependent AP shortening of hiPSC-CM to $I_{Ca,L}$ and I_{Kr} dynamics. AP shortening upon I_{K1} injection has indeed been shown previously in native cardiomyocytes [72], in hiPSC-CMs [4, 70], and in silico models [14]. To our knowledge, we provide the first evidence of maturation-induced I_{K1} mediation of APD shortening in hiPSC-CM. This finding, along with our accompanying iMATURE maturation simulation software, could provide insight into the heterogeneous AP profiles which are regularly reported within and between hiPSC-CM cohorts. Future innovative studies promoting hiPSC-CM maturation should focus similarly on I_{K1} development as this will be a key component in optimising hiPSC-CM for widespread screening initiatives [25].

Potential implications

Inherent variability in hiPSC-CM function hinders reliable quantification of average behaviour. In silico modelling has emerged as a powerful solution to link dispersed data sets and precisely define cellular parameters that contribute to experimentally observed heterogeneity. The recent state-of-the-art Kernik hiPSC-CM model integrates a wide range of experimental data by building a predictive array of cellular variability that allows for detailed investigation of cellular electrophysiology and underlying causal mechanisms of phenotypical heterogeneity [36]. Despite the availability of several useful hiPSC-CM models, none has comprehensively considered the ages of the hiPSC-CM used in the underlying experimental data. Using our own experimental findings and the framework of the Kernik model, we present the first hiPSC-CM model in which minimal parameter change can reproduce a wide range of electrophysiological properties of early- and late-stage hiPSC-CM (Online Figs. S4–S8). To facilitate analyses of maturation-dependent effects, our model has been integrated into an open-source interface, iMATURE, which allows the user to manually select the age of hiPSC-CM post differentiation and receive predictive readouts of AP morphology and ion channel dynamics over their specified age range. This platform also allows for manual modulation of individual ion channels and Ca^{2+} fluxes at any cellular age between 21 and 80 days post differentiation, enabling the investigation of age-dependent responses to hypothetical cardiotropic compounds (Fig. 8). Increased understanding of the impact of time-dependent phenotypic changes in hiPSC-CM is expected to contribute to standardisation of methodological techniques. Accordingly, this may enhance the quality of hiPSC-CM platforms, reduce variability in functional readouts, and promote efficient outlets for personalised medicine and streamline drug development [21].

Potential limitations

In addition to prolonged cultivation times, strategies to enhance hiPSC-CM maturity include the adoption of appropriate cardiac differentiation protocols [6], culture substrates [23] and the application of mechanical, chemical or electrical stress to hiPSC-CM embedded in 3D hydrogels or fibrin blocks to more closely replicate the in vivo environment [35, 57, 68]. From an electrophysiological point of view, 2D cultivation strategies seem to be particularly limited with respect to the slow upstroke velocity of the AP, which is a common finding in all studies (Table 1). In contrast, 3D culture strategies seem to provide a promising improvement showing faster AP upstroke velocities (Table 2) [46]. It is important to note that the concept of hiPSC-CM maturation is a broad paradigm which also encompasses molecular, metabolic and structural properties [47]. Previous reports of hiPSC-CM maturation indeed show structural elongation and heightened sarcomere organisation, resembling the classical rod shape of cardiomyocytes [33, 49]. We observed highly heterogeneous morphological features in our developing cellular cultures with both rod-like and rounded cells. Measuring individual cells in sparsely seeded monolayers is essential for gathering true electrophysiological readouts; however, this environment is inherently artificial due to severely decreased cell-to-cell communication. Therefore, various external paracrine effects and electrical stimuli may not play a major role in the development of our cells [37]. Our differentiation technique enables a baseline assessment of cellular function under fully defined culture conditions. Further studies using targeted maturation-enhancing techniques can, therefore, build upon this foundation.

In addition to the remodelling characterised in the present study, other currents may contribute to hiPSC-CM electrical development and age-dependent action potential shortening. Cardiac currents such as *t*-type calcium current ($I_{Ca,T}$), I_f, transient-outward K^+ current (I_{to}) or the slow component of the delayed-rectifier K^+ current (I_{Ks}) were not experimentally quantified, although they are present within the Kernik hiPSC-CM computer model [36] that our work is based on. Previous studies have identified a large role for I_{Ks} and I_{Kr} in the maintenance of repolarization reserve in adult human cardiomyocytes [5, 32]. During our experimental examination of I_{K1} block on AP duration, we cannot exclude the possibility that our high concentration of $BaCl_2$ could also cause unspecific inhibition of the delayed-rectifier K^+ currents [32]. Following consolidation with our entire experimental data set, our iMATURE platform is able to provide appropriate readouts of all cardiac-related currents and does not indicate a strong contribution of the delayed-rectifier K^+ currents in age-related AP shortening in hiPSC-CM.

hiPSC-CMs also show regional subtype-specific traits that allow them to be classified as ventricular-, atrial- or nodal-like cardiomyocytes [29]. In the absence of an intervention to direct subtype differentiation, for example by promoting an atrial phenotype with retinoic acid, hiPSC-CM generally show predominantly ventricular traits, with minimal mixing of other subtypes [10]. We cannot definitively state that our experimental data contains only ventricular-like cells. Differences in ionic makeup of atrial and nodal cells influence their AP morphology and repolarisation profile, which are, therefore, commonly utilised as functional markers of cellular subtype [13]. The repolarisation fraction provides an index of phase 3 AP kinetics and, in our hands, does not show evidence of atrial or nodal cell contamination in our experimental cohort. In addition, no significant change in repolarisation fraction was detected during maturation, indicating the absence of a subtype-shift during prolonged culture as has been recently proposed [3].

Additionally, some potential limitations should be considered related to the computational modelling performed in this study. (1) Although we employed a widely used and well-validated state-of-the-art in silico model of hiPSC-CM [36], the model dependence of our results cannot be excluded. (2) The intercellular heterogeneity of ion channel distribution and activity could potentially affect our observed AP properties. Here, we present a single deterministic hiPSC-CM model without intercellular variability. Although we do identify an overall trend of age-dependent AP shortening in hiPSC-CM, future research should employ high-throughput electrophysiological techniques and multiple populations of in silico hiPSC-CM models to properly capture and map this phenomenon.

Conclusions

In this study we have shown that hiPSC-CM under standard and simplified culture conditions show distinct alterations in electrical function and Ca^{2+} handling over extended time periods. Key ionic currents such as $I_{Ca,L}$ and I_{K1}, crucial for homeostatic cellular function, show increased functional expression in older hiPSC-CM cultures, with the latter likely contributing to maturation-dependent AP shortening. Our experimental data fit well within established in silico frameworks, and our new user interface software allows for easy and rapid analysis of an optimal temporal 'window' in which disease modelling or assessments of proarrhythmic risk can be effectively performed, thus minimising heterogeneity between functional readouts.

Supplementary Information The online version contains supplementary material available at https://doi.org/10.1007/s00395-022-00973-0.

Acknowledgements The authors thank Laura Cyganek, Nadine Gotzmann, Yvonne Hintz, Lisa Krebs, Yvonne Wedekind (all Stem Cell Unit, UMG), Regina Beushausen, Joanna Heide, Stefanie Kestel and Ines Müller (UMG) for their exemplary assistance and Maren Dilaj for excellent secretarial help.

Author contributions FS, HS, TR, FEF, FEM, JH and NV designed the studies. FS, HS, RD, JRDP, MRap, RS, AL, MRit, PJ, LS, LMH, MK, NH, SP, JH and NV performed the research and analysed the data. SP, KSB, LC, and SS provided cellular material and analysis expertise. FS, HS, JH and NV wrote the manuscript. All authors give their consent for the publication of the above manuscript.

Funding Open Access funding enabled and organized by Projekt DEAL. This work was supported by grants from the Deutsche Forschungsgemeinschaft (DFG) to NV (VO 1568/3-1, VO1568/4-1, IRTG1816, SFB1002 project A13 and under Germany's Excellence Strategy—EXC 2067/1—390729940), from the Else-Kröner-Fresenius Foundation to NV (EKFS 2016_A20) and KSB and SS (EKFS 2017_A137), from the German Center for Cardiovascular Research to NV (DZHK 81X4300102, 81X4300115, 81X4300112), and by the Netherlands Organization for Scientific Research to JH (NWO/ZonMW Vidi 09150171910029).

Data availability All available data are incorporated into this article and its online supplementary material. iMATURE and Myokit are both freely available and can be downloaded from the authors' websites (www.github.com/jordiheijman and http://www.myokit.org). Detailed installation instructions are provided in the Online Supplement.

Declarations

Conflict of interest Markus Rapedius is an employee of Nanion Technologies GmbH. The authors have no further conflicts of interest to declare.

Ethical approval This study was performed in line with the principles of the Declaration of Helsinki. Approval was granted by the Ethics Committee of University Medical Center Göttingen (10/9/15).

References

1. Anson BD, Kolaja KL, Kamp TJ (2011) Opportunities for use of human iPS cells in predictive toxicology. Clin Pharmacol Ther 89:754–758. https://doi.org/10.1038/clpt.2011.9
2. Bailly P, Mouchonière M, Bénitah JP, Camilleri L, Vassort G, Lorente P (1998) Extracellular K^+ dependence of inward rectification kinetics in human left ventricular cardiomyocytes. Circulation 98:2753–2759. https://doi.org/10.1161/01.cir.98.24.2753
3. Ben-Ari M, Naor S, Zeevi-Levin N, Schick R, Ben Jehuda R, Reiter I, Raveh A, Grijnevitch I, Barak O, Rosen MR, Weissman A, Binah O (2016) Developmental changes in electrophysiological characteristics of human-induced pluripotent stem cell-derived cardiomyocytes. Hear Rhythm 13:2379–2387. https://doi.org/10.1016/j.hrthm.2016.08.045
4. Bett GCL, Kaplan AD, Lis A, Cimato TR, Tzanakakis ES, Zhou Q, Morales MJ, Rasmusson RL (2013) Electronic "expression" of the inward rectifier in cardiocytes derived from human-induced pluripotent stem cells. Hear Rhythm 10:1903–1910. https://doi.org/10.1016/j.hrthm.2013.09.061
5. Biliczki P, Virág L, Iost N, Papp JG, Varró A (2002) Interaction of different potassium channels in cardiac repolarization in dog ventricular preparations: role of repolarization reserve. Br J Pharmacol 137:361–368. https://doi.org/10.1038/sj.bjp.0704881
6. Burridge PW, Matsa E, Shukla P, Lin ZC, Churko JM, Ebert AD, Lan F, Diecke S, Huber B, Mordwinkin NM, Plews JR, Abilez OJ, Cui B, Gold JD, Wu JC (2014) Chemically defined generation of human cardiomyocytes. Nat Methods 11:855–860. https://doi.org/10.1038/nmeth.2999
7. Casini S, Verkerk AO, Remme CA (2017) Human iPSC-derived cardiomyocytes for investigation of disease mechanisms and therapeutic strategies in inherited arrhythmia syndromes: strengths and limitations. Cardiovasc Drugs Ther 31:325–344. https://doi.org/10.1007/s10557-017-6735-0
8. Christ T, Rozmaritsa N, Engel A, Berk E, Knaut M, Metzner K, Canteras M, Ravens U, Kaumann A (2014) Arrhythmias, elicited by catecholamines and serotonin, vanish in human chronic atrial fibrillation. PNAS 111:11193–11198. https://doi.org/10.1073/pnas.1324132111
9. Clerx M, Collins P, de Lange E, Volders PGA (2016) Myokit: A simple interface to cardiac cellular electrophysiology. Prog Biophys Mol Biol 120:100–114. https://doi.org/10.1016/j.pbiomolbio.2015.12.008
10. Cyganek L, Tiburcy M, Sekeres K, Gerstenberg K, Bohnenberger H, Lenz C, Henze S, Stauske M, Salinas G, Zimmermann W-H, Hasenfuss G, Guan K (2018) Deep phenotyping of human induced pluripotent stem cell-derived atrial and ventricular cardiomyocytes. JCI insight. https://doi.org/10.1172/jci.insight.99941
11. Dolnikov K, Shilkrut M, Zeevi-Levin N, Gerecht-Nir S, Amit M, Danon A, Itskovitz-Eldor J, Binah O (2006) Functional properties of human embryonic stem cell-derived cardiomyocytes: intracellular Ca^{2+} handling and the role of sarcoplasmic reticulum in the contraction. Stem Cells 24:236–245. https://doi.org/10.1634/stemcells.2005-0036
12. Doss MX, Di Diego JM, Goodrow RJ, Wu Y, Cordeiro JM, Nesterenko VV, Barajas-Martínez H, Hu D, Urrutia J, Desai M, Treat JA, Sachinidis A, Antzelevitch C (2012) Maximum diastolic potential of human induced pluripotent stem cell-derived cardiomyocytes depends critically on I_{Kr}. PLoS ONE. https://doi.org/10.1371/journal.pone.0040288
13. Du DTM, Hellen N, Kane C, Terracciano CMN (2015) Action potential morphology of human induced pluripotent stem cell-derived cardiomyocytes does not predict cardiac chamber specificity and is dependent on cell density. Biophys J 108:1–4. https://doi.org/10.1016/j.bpj.2014.11.008
14. Fabbri A, Goversen B, Vos MA, van Veen TAB, de Boer TP (2019) Required G_{K1} to suppress automaticity of iPSC-CMs depends strongly on I_{K1} model structure. Biophys J 117:2303–2315. https://doi.org/10.1016/j.bpj.2019.08.040
15. Fakuade FE, Steckmeister V, Seibertz F, Gronwald J, Kestel S, Menzel J, Pronto JRD, Taha K, Haghighi F, Kensah G, Pearman CM, Wiedmann F, Teske AJ, Schmidt C, Dibb KM, El-Essawi A, Danner BC, Baraki H, Schwappach B, Kutschka I, Mason FE, Voigt N (2020) Altered atrial cytosolic calcium handling contributes to the development of postoperative atrial

fibrillation. Cardiovasc Res. https://doi.org/10.1093/cvr/cvaa162
16. Fauconnier J, Lacampagne A, Rauzier J-M, Vassort G, Richard S (2005) Ca^{2+}-dependent reduction of I_{K1} in rat ventricular cells: A novel paradigm for arrhythmia in heart failure? Cardiovasc Res 68:204–212. https://doi.org/10.1016/j.cardiores.2005.05.024
17. Fermini B, Hancox JC, Abi-Gerges N, Bridgland-Taylor M, Chaudhary KW, Colatsky T, Correll K, Crumb W, Damiano B, Erdemli G, Gintant G, Imredy J, Koerner J, Kramer J, Levesque P, Li Z, Lindqvist A, Obejero-Paz CA, Rampe D, Sawada K, Strauss DG, Vandenberg JI (2016) A new perspective in the field of cardiac safety testing through the comprehensive in vitro proarrhythmia assay paradigm. J Biomol Screen 21:1–11. https://doi.org/10.1177/1087057115594589
18. Goversen B, Becker N, Stoelzle-Feix S, Obergrussberger A, Vos MA, van Veen TAB, Fertig N, de Boer TP (2018) A hybrid model for safety pharmacology on an automated patch clamp platform: using dynamic clamp to join iPSC-derived cardiomyocytes and simulations of I_{K1} ion channels in real-time. Front Physiol 8:1094
19. Hanses U, Kleinsorge M, Roos L, Yigit G, Li Y, Barbarics B, El-Battrawy I, Lan H, Tiburcy M, Hindmarsh R, Lenz C, Salinas G, Diecke S, Müller C, Adham I, Altmüller J, Nürnberg P, Paul T, Zimmermann WH, Hasenfuss G, Wollnik B, Cyganek L (2020) Intronic CRISPR repair in a preclinical model of noonan syndrome-associated cardiomyopathy. Circulation 142:1059–1076. https://doi.org/10.1161/CIRCULATIONAHA.119.044794
20. Hartmann N, Pabel S, Herting J, Schatter F, Renner A, Gummert J, Schotola H, Danner BC, Maier LS, Frey N, Hasenfuss G, Fischer TH, Sossalla S (2017) Antiarrhythmic effects of dantrolene in human diseased cardiomyocytes. Hear Rhythm 14:412–419. https://doi.org/10.1016/j.hrthm.2016.09.014
21. Heijman J, Voigt N, Carlsson LG, Dobrev D (2014) Cardiac safety assays. Curr Opin Pharmacol 15:16–21. https://doi.org/10.1016/j.coph.2013.11.004
22. Heijman J, Voigt N, Wehrens XHT, Dobrev D (2014) Calcium dysregulation in atrial fibrillation: the role of CaMKII. Front Pharmacol 5:30. https://doi.org/10.3389/fphar.2014.00030
23. Herron TJ, Da Rocha AM, Campbell KF, Ponce-Balbuena D, Willis BC, Guerrero-Serna G, Liu Q, Klos M, Musa H, Zarzoso M, Bizy A, Furness J, Anumonwo J, Mironov S, Jalife J (2016) Extracellular matrix-mediated maturation of human pluripotent stem cell-derived cardiac monolayer structure and electrophysiological function. Circ Arrhythmia Electrophysiol 9:1–13. https://doi.org/10.1161/CIRCEP.113.003638
24. Hoekstra M, Mummery C, Wilde A, Bezzina C, Verkerk A (2012) Induced pluripotent stem cell derived cardiomyocytes as models for cardiac arrhythmias. Front Physiol 3:346
25. Horváth A, Lemoine MD, Löser A, Mannhardt I, Flenner F, Uzun AU, Neuber C, Breckwoldt K, Hansen A, Girdauskas E, Reichenspurner H, Willems S, Jost N, Wettwer E, Eschenhagen T, Christ T (2018) Low resting membrane potential and low inward rectifier potassium currents are not inherent features of hiPSC-derived cardiomyocytes. Stem Cell Reports 10:822–833. https://doi.org/10.1016/j.stemcr.2018.01.012
26. Huang M, Liao Z, Li X, Yang Z, Fan X, Li Y, Zhao Z, Lang S, Cyganek L, Zhou X, Akin I, Borggrefe M, El-Battrawy I (2021) Effects of antiarrhythmic drugs on hERG gating in human-induced pluripotent stem cell-derived cardiomyocytes from a patient with short QT syndrome type 1. Front Pharmacol 12:675003. https://doi.org/10.3389/fphar.2021.675003
27. Hwang HS, Kryshtal DO, Feaster TK, Sánchez-Freire V, Zhang J, Kamp TJ, Hong CC, Wu JC, Knollmann BC (2015) Comparable calcium handling of human iPSC-derived cardiomyocytes generated by multiple laboratories. J Mol Cell Cardiol 85:79–88. https://doi.org/10.1016/j.yjmcc.2015.05.003
28. Iost N, Virág L, Opincariu M, Szécsi J, Varró A, Papp JG (1998) Delayed rectifier potassium current in undiseased human ventricular myocytes. Cardiovasc Res 40:508–515. https://doi.org/10.1016/s0008-6363(98)00204-1
29. Itzhaki I, Maizels L, Huber I, Zwi-Dantsis L, Caspi O, Winterstern A, Feldman O, Gepstein A, Arbel G, Hammerman H, Boulos M, Gepstein L (2011) Modelling the long QT syndrome with induced pluripotent stem cells. Nature 471:225–229. https://doi.org/10.1038/nature09747
30. Jeck CD, Boyden PA (1992) Age-related appearance of outward currents may contribute to developmental differences in ventricular repolarization. Circ Res 71:1390–1403. https://doi.org/10.1161/01.res.71.6.1390
31. Jonsson MKB, Vos MA, Mirams GR, Duker G, Sartipy P, de Boer TP, van Veen TAB (2012) Application of human stem cell-derived cardiomyocytes in safety pharmacology requires caution beyond hERG. J Mol Cell Cardiol 52:998–1008. https://doi.org/10.1016/j.yjmcc.2012.02.002
32. Jost N, Virág L, Comtois P, Ordög B, Szuts V, Seprényi G, Bitay M, Kohajda Z, Koncz I, Nagy N, Szél T, Magyar J, Kovács M, Puskás LG, Lengyel C, Wettwer E, Ravens U, Nánási PP, Papp JG, Varró A, Nattel S (2013) Ionic mechanisms limiting cardiac repolarization reserve in humans compared to dogs. J Physiol 591:4189–4206. https://doi.org/10.1113/jphysiol.2013.261198
33. Kamakura T, Makiyama T, Sasaki K, Yoshida Y, Wuriyanghai Y, Chen J, Hattori T, Ohno S, Kita T, Horie M, Yamanaka S, Kimura T (2013) Ultrastructural maturation of human-induced pluripotent stem cell-derived cardiomyocytes in a long-term culture. Circ J 77:1307–1314. https://doi.org/10.1253/circj.CJ-12-0987
34. Karakikes I, Ameen M, Termglinchan V, Wu JC (2015) Human induced pluripotent stem cell-derived cardiomyocytes: insights into molecular, cellular, and functional phenotypes. Circ Res 117:80–88. https://doi.org/10.1161/CIRCRESAHA.117.305365
35. Kensah G, Lara AR, Dahlmann J, Zweigerdt R, Schwanke K, Hegermann J, Skvorc D, Gawol A, Azizian A, Wagner S, Maier LS, Krause A, Dräger G, Ochs M, Haverich A, Gruh I, Martin U (2013) Murine and human pluripotent stem cell-derived cardiac bodies form contractile myocardial tissue in vitro. Eur Heart J 34:1134–1146. https://doi.org/10.1093/eurheartj/ehs349
36. Kernik DC, Morotti S, Wu H, Garg P, Duff HJ, Kurokawa J, Jalife J, Wu JC, Grandi E, Clancy CE (2019) A computational model of induced pluripotent stem-cell derived cardiomyocytes incorporating experimental variability from multiple data sources. J Physiol 597:4533–4564. https://doi.org/10.1113/JP277724
37. Kim C, Majdi M, Xia P, Wei KA, Talantova M, Spiering S, Nelson B, Mercola M, Chen HV (2009) Non-cardiomyocytes influence the electrophysiological maturation of human embryonic stem cell-derived cardiomyocytes during differentiation. Stem Cells Dev 19:783–795. https://doi.org/10.1089/scd.2009.0349
38. Kim JJ, Yang L, Lin B, Zhu X, Sun B, Kaplan AD, Bett GCL, Rasmusson RL, London B, Salama G (2015) Mechanism of automaticity in cardiomyocytes derived from human induced pluripotent stem cells. J Mol Cell Cardiol 81:81–93. https://doi.org/10.1016/j.yjmcc.2015.01.013
39. Kleinsorge M, Cyganek L (2020) Subtype-directed differentiation of human iPSCs into atrial and ventricular cardiomyocytes. STAR Protoc. https://doi.org/10.1016/j.xpro.2020.100026
40. Koivumäki JT, Naumenko N, Tuomainen T, Takalo J, Oksanen M, Puttonen KA, Lehtonen Š, Kuusisto J, Laakso M, Koistinaho J, Tavi P (2018) Structural immaturity of human iPSC-derived cardiomyocytes: in silico investigation of effects on function and disease modeling. Front Physiol 9:80. https://doi.org/10.3389/fphys.2018.00080

41. Konarzewska H, Peeters GA, Sanguinetti MC (1995) Repolarizing K^+ currents in nonfailing human hearts. Similarities between right septal subendocardial and left subepicardial ventricular myocytes. Circulation 92:1179–1187. https://doi.org/10.1161/01.cir.92.5.1179
42. Koumi S, Backer CL, Arentzen CE, Sato R (1995) beta-Adrenergic modulation of the inwardly rectifying potassium channel in isolated human ventricular myocytes. Alteration in channel response to beta-adrenergic stimulation in failing human hearts. J Clin Invest 96:2870–2881. https://doi.org/10.1172/JCI118358
43. Lee S, Lee H-A, Choi SW, Kim SJ, Kim K-S (2016) Evaluation of nefazodone-induced cardiotoxicity in human induced pluripotent stem cell-derived cardiomyocytes. Toxicol Appl Pharmacol 296:42–53. https://doi.org/10.1016/j.taap.2016.01.015
44. Lee Y-K, Ng K-M, Lai W-H, Chan Y-C, Lau Y-M, Lian Q, Tse H-F, Siu C-W (2011) Calcium homeostasis in human induced pluripotent stem cell-derived cardiomyocytes. Stem Cell Rev Reports 7:976–986. https://doi.org/10.1007/s12015-011-9273-3
45. Lemoine MD, Krause T, Koivumäki JT, Prondzynski M, Schulze ML, Girdauskas E, Willems S, Hansen A, Eschenhagen T, Christ T (2018) Human induced pluripotent stem cell-derived engineered heart tissue as a sensitive test system for QT prolongation and arrhythmic triggers. Circ Arrhythm Electrophysiol 11:e006035. https://doi.org/10.1161/CIRCEP.117.006035
46. Lemoine MD, Mannhardt I, Breckwoldt K, Prondzynski M, Flenner F, Ulmer B, Hirt MN, Neuber C, Horváth A, Kloth B, Reichenspurner H, Willems S, Hansen A, Eschenhagen T, Christ T (2017) Human iPSC-derived cardiomyocytes cultured in 3D engineered heart tissue show physiological upstroke velocity and sodium current density. Sci Rep 7:5464. https://doi.org/10.1038/s41598-017-05600-w
47. Liaw NY, Zimmermann W-H (2016) Mechanical stimulation in the engineering of heart muscle. Adv Drug Deliv Rev 96:156–160. https://doi.org/10.1016/j.addr.2015.09.001
48. Liu J, Fu JD, Siu CW, Li RA (2007) Functional sarcoplasmic reticulum for calcium handling of human embryonic stem cell-derived cardiomyocytes: insights for driven maturation. Stem Cells 25:3038–3044. https://doi.org/10.1634/stemcells.2007-0549
49. Lundy SD, Zhu W-Z, Regnier M, Laflamme MA (2013) Structural and functional maturation of cardiomyocytes derived from human pluripotent stem cells. Stem Cells Dev 22:1991–2002. https://doi.org/10.1089/scd.2012.0490
50. Ma J, Guo L, Fiene SJ, Anson BD, Thomson JA, Kamp TJ, Kolaja KL, Swanson BJ, January CT (2011) High purity human-induced pluripotent stem cell-derived cardiomyocytes: electrophysiological properties of action potentials and ionic currents. Am J Physiol Heart Circ Physiol 301:H2006–H2017. https://doi.org/10.1152/ajpheart.00694.2011
51. Magyar J, Iost N, Körtvély A, Bányász T, Virág L, Szigligeti P, Varró A, Opincariu M, Szécsi J, Papp JG, Nánási PP (2000) Effects of endothelin-1 on calcium and potassium currents in undiseased human ventricular myocytes. Pflugers Arch 441:144–149. https://doi.org/10.1007/s004240000400
52. Meijer van Putten RME, Mengarelli I, Guan K, Zegers JG, van Ginneken ACG, Verkerk AO, Wilders R (2015) Ion channelopathies in human induced pluripotent stem cell derived cardiomyocytes: a dynamic clamp study with virtual I_{K1}. Front Physiol 6:7
53. Mewes T, Ravens U (1994) L-type calcium currents of human myocytes from ventricle of non-failing and failing hearts and from atrium. J Mol Cell Cardiol 26:1307–1320. https://doi.org/10.1006/jmcc.1994.1149
54. Paci M, Hyttinen J, Aalto-Setälä K, Severi S (2013) Computational models of ventricular- and atrial-like human induced pluripotent stem cell derived cardiomyocytes. Ann Biomed Eng 41:2334–2348. https://doi.org/10.1007/s10439-013-0833-3
55. Paci M, Pölönen R-P, Cori D, Penttinen K, Aalto-Setälä K, Severi S, Hyttinen J (2018) Automatic optimization of an in silico model of human iPSC derived cardiomyocytes recapitulating calcium handling abnormalities. Front Physiol 9:709. https://doi.org/10.3389/fphys.2018.00709
56. Poulet C, Wettwer E, Grunnet M, Jespersen T, Fabritz L, Matschke K, Knaut M, Ravens U (2015) Late sodium current in human atrial cardiomyocytes from patients in sinus rhythm and atrial fibrillation. PLoS ONE 10:e0131432. https://doi.org/10.1371/journal.pone.0131432
57. Radisic M, Park H, Shing H, Consi T, Schoen FJ, Langer R, Freed LE, Vunjak-novakovic G (2004) Functional assembly of engineered myocardium by electrical stimulation of cardiac myocytes cultured on scaffolds. PNAS 101:18129–18134
58. Reppel M, Fleischmann BK, Reuter H, Sasse P, Schunkert H, Hescheler J (2007) Regulation of the Na^+/Ca^{2+} exchanger (NCX) in the murine embryonic heart. Cardiovasc Res 75:99–108. https://doi.org/10.1016/j.cardiores.2007.03.018
59. Rössler U, Hennig AF, Stelzer N, Bose S, Kopp J, Søe K, Cyganek L, Zifarelli G, Ali S, von der Hagen M, Strässler ET, Hahn G, Pusch M, Stauber T, Izsvák Z, Gossen M, Stachelscheid H, Kornak U (2021) Efficient generation of osteoclasts from human induced pluripotent stem cells and functional investigations of lethal CLCN7-related osteopetrosis. J bone Miner Res 36:1621–1635. https://doi.org/10.1002/jbmr.4322
60. Sager PT, Gintant G, Turner JR, Pettit S, Stockbridge N (2014) Rechanneling the cardiac proarrhythmia safety paradigm: a meeting report from the Cardiac Safety Research Consortium. Am Heart J 167:292–300
61. Sakakibara Y, Furukawa T, Singer DH, Jia H, Backer CL, Arentzen CE, Wasserstrom JA (1993) Sodium current in isolated human ventricular myocytes. Am J Physiol 265:H1301–H1309. https://doi.org/10.1152/ajpheart.1993.265.4.H1301
62. Sala L, van Meer BJ, Tertoolen LGJ, Bakkers J, Bellin M, Davis RP, Denning C, Dieben MAE, Eschenhagen T, Giacomelli E, Grandela C, Hansen A, Holman ER, Jongbloed MRM, Kamel SM, Koopman CD, Lachaud Q, Mannhardt I, Mol MPH, Mosqueira D, Orlova VV, Passier R, Ribeiro MC, Saleem U, Smith GL, Burton FL, Mummery CL (2018) Musclemotion: a versatile open software tool to quantify cardiomyocyte and cardiac muscle contraction in vitro and in vivo. Circ Res 122:e5–e16. https://doi.org/10.1161/CIRCRESAHA.117.312067
63. Sala L, Yu Z, Ward-van Oostwaard D, van Veldhoven JP, Moretti A, Laugwitz K-L, Mummery CL, IJzerman AP, Bellin M, (2016) A new hERG allosteric modulator rescues genetic and drug-induced long-QT syndrome phenotypes in cardiomyocytes from isogenic pairs of patient induced pluripotent stem cells. EMBO Mol Med 8:1065–1081. https://doi.org/10.15252/emmm.201606260
64. Sartiani L, Bettiol E, Stillitano F, Mugelli A, Cerbai E, Jaconi ME (2007) Developmental changes in cardiomyocytes differentiated from human embryonic stem cells: a molecular and electrophysiological approach. Stem Cells 25:1136–1144. https://doi.org/10.1634/stemcells.2006-0466
65. Schönherr R, Heinemann SH (1996) Molecular determinants for activation and inactivation of HERG, a human inward rectifier potassium channel. J Physiol 493(Pt 3):635–642. https://doi.org/10.1113/jphysiol.1996.sp021410
66. Sun Y, Timofeyev V, Dennis A, Bektik E, Wan X, Laurita KR, Deschênes I, Li RA, Fu J-D (2017) A singular role of I_{K1} promoting the development of cardiac automaticity during cardiomyocyte differentiation by I_{K1}—induced activation of pacemaker current. Stem Cell Rev Reports 13:631–643. https://doi.org/10.1007/s12015-017-9745-1
67. Sutanto H, Lyon A, Lumens J, Schotten U, Dobrev D, Heijman J (2020) Cardiomyocyte calcium handling in health and disease:

Insights from in vitro and in silico studies. Prog Biophys Mol Biol. https://doi.org/10.1016/j.pbiomolbio.2020.02.008
68. Tiburcy M, Hudson JE, Balfanz P, Schlick S, Meyer T, Chang Liao M-L, Levent E, Raad F, Zeidler S, Wingender E, Riegler J, Wang M, Gold JD, Kehat I, Wettwer E, Ravens U, Dierickx P, van Laake LW, Goumans MJ, Khadjeh S, Toischer K, Hasenfuss G, Couture LA, Unger A, Linke WA, Araki T, Neel B, Keller G, Gepstein L, Wu JC, Zimmermann W-H (2017) Defined engineered human myocardium with advanced maturation for applications in heart failure modeling and repair. Circulation 135:1832–1847. https://doi.org/10.1161/CIRCULATIONAHA.116.024145
69. Valdivia CR, Chu WW, Pu J, Foell JD, Haworth RA, Wolff MR, Kamp TJ, Makielski JC (2005) Increased late sodium current in myocytes from a canine heart failure model and from failing human heart. J Mol Cell Cardiol 38:475–483. https://doi.org/10.1016/j.yjmcc.2004.12.012
70. van Putten RME, Mengarelli I, Guan K, Zegers JG, van Ginneken ACG, Verkerk AO, Wilders R (2015) Ion channelopathies in human induced pluripotent stem cell derived cardiomyocytes: a dynamic clamp study with virtual I_{K1}. Front Physiol 6:7. https://doi.org/10.3389/fphys.2015.00007
71. Veerman CC, Mengarelli I, Guan K, Stauske M, Barc J, Tan HL, Wilde AAM, Verkerk AO, Bezzina CR (2016) hiPSC-derived cardiomyocytes from Brugada Syndrome patients without identified mutations do not exhibit clear cellular electrophysiological abnormalities. Sci Rep 6:30967. https://doi.org/10.1038/srep30967
72. Verkerk AO, Veldkamp MW, de Jonge N, Wilders R, van Ginneken ACG (2000) Injury current modulates afterdepolarizations in single human ventricular cells. Cardiovasc Res 47:124–132. https://doi.org/10.1016/S0008-6363(00)00064-X
73. Voigt N, Heijman J, Wang Q, Chiang DY, Li N, Karck M, Wehrens XHT, Nattel S, Dobrev D (2014) Cellular and molecular mechanisms of atrial arrhythmogenesis in patients with paroxysmal atrial fibrillation. Circulation 129:145–156. https://doi.org/10.1161/CIRCULATIONAHA.113.006641
74. Voigt N, Li N, Wang Q, Wang W, Trafford AW, Abu-Taha I, Sun Q, Wieland T, Ravens U, Nattel S, Wehrens XHT, Dobrev D (2012) Enhanced sarcoplasmic reticulum Ca^{2+} Leak and increased Na^{+}–Ca^{2+} exchanger function underlie delayed afterdepolarizations in patients with chronic atrial fibrillation. Circulation 125:2059–2070. https://doi.org/10.1161/CIRCULATIONAHA.111.067306
75. Voigt N, Pearman CM, Dobrev D, Dibb KM (2015) Methods for isolating atrial cells from large mammals and humans. J Mol Cell Cardiol 86:187–198. https://doi.org/10.1016/j.yjmcc.2015.07.006
76. Voigt N, Trausch A, Knaut M, Matschke K, Varró A, Van Wagoner DR, Nattel S, Ravens U, Dobrev D (2010) Left-to-right atrial inward rectifier potassium current gradients in patients with paroxysmal versus chronic atrial fibrillation. Circ Arrhythmia Electrophysiol 3:472–480. https://doi.org/10.1161/CIRCEP.110.954636
77. Voigt N, Zhou X-B, Dobrev D (2013) Isolation of human atrial myocytes for simultaneous measurements of Ca^{2+} transients and membrane currents. J Vis Exp. https://doi.org/10.3791/50235
78. Walden AP, Dibb KM, Trafford AW (2009) Differences in intracellular calcium homeostasis between atrial and ventricular myocytes. J Mol Cell Cardiol 46:463–473. https://doi.org/10.1016/j.yjmcc.2008.11.003
79. Yoshida Y, Yamanaka S (2017) Induced pluripotent stem cells 10 years later for cardiac applications. Circ Res 120:1958–1969. https://doi.org/10.1161/CIRCRESAHA.117.311080
80. Zaza A, Rocchetti M, Brioschi A, Cantadori A, Ferroni A (1998) Dynamic Ca^{2+}-induced inward rectification of K^{+} current during the ventricular action potential. Circ Res 82:947–956. https://doi.org/10.1161/01.RES.82.9.947
81. Zhao Z, Lan H, El-Battrawy I, Li X, Buljubasic F, Sattler K, Yücel G, Lang S, Tiburcy M, Zimmermann W-H, Cyganek L, Utikal J, Wieland T, Borggrefe M, Zhou X-B, Akin I (2018) Ion channel expression and characterization in human induced pluripotent stem cell-derived cardiomyocytes. Stem Cells Int 2018:6067096. https://doi.org/10.1155/2018/6067096